**MINISTRY OF EDUCATION AND TRAINING**

**VIETNAM ACADEMY OF SCIENCE AND TECHNOLOGY**

**INSTITUTE OF PHYSICS**

**PHAM TUAN ANH**

# RADIO DETECTION OF THE SUN

**MASTER THESIS**
**ATOMIC, NUCLEAR AND PARTICLE PHYSICS**
**CODE: 60.44.05**

**SUPERVISOR: PROF. PIERRE DARRIULAT**

**HANOI - 2010**

# ACKNOWLEDGEMENTS

The present work was performed at the Vietnam Auger Training Laboratory (VATLY), in the Institute of Nuclear Science and Technology (INST) under the supervision of Professor Pierre Darriulat. Pierre was always here to listen to my difficulties and to give his support. He is responsible for having involved me in this project. He taught me how to ask questions and express my ideas. He showed me the ways to approach a research problem and the need to be persistent to accomplish the task. My view about science has changed after having worked with him. I owe him my deepest gratitude.

This work would not have been possible without the precious support of Dr. Dang Quang Thieu. I am deeply indebted to him for having provided me with many essential tools: a 30 MHz generator, a 30 MHz amplifier, an 8-bit ADC, a frequency meter, etc. I was always welcome in his electronics lab when I had to fix faulty units and he would patiently guide me and give me advice.

I thank warmly those who gave us encouragement, help and support and, in particular, Professor Academician Nguyen Van Hieu, Professor Nguyen Quang Rieu, at the origin of this initiative and Professor Dinh Van Trung whose support has been invaluable.

I gratefully thank Drs Nguyen Phuc, F. Biraud, B. Darchy, Tran Trong My, Tran Minh Van and Nguyen Thi Bao My, who gave me technical help and advice or allowed me to use some of their measuring equipment.

A special thank goes to Ms Hoang Mai Anh for her generous hospitality in her beautiful Hoa Binh villa where we could collect data conveniently. I also should like to thank Ms Nguyen Thi Nga who took care of us on these occasions.

I would like to express my gratitude to Dr. Vo Van Thuan for his strong and continued support.

It is a pleasure to thank the members of the VATLY team who made this thesis possible, among which Pham Ngoc Dong and Pham Thi Tuyet Nhung deserve a special mention. They shared with me their working experience and helped me whenever I was in trouble.

I acknowledge financial support from the Vietnamese Ministry of Science and Technology and from the World Laboratory.

CONTENT

# INTRODUCTION

Radio astronomy was born less than a century ago and has since developed into one of the most successful branches of modern astrophysics. While, apart for a narrow window in the visible, higher frequency electromagnetic radiations are absorbed by the Earth atmosphere, radio waves reach the Earth essentially undisturbed. As a consequence, and at variance with other branches of modern astrophysics, radio astronomy observations are made from ground. Moreover, as the wavelengths being used are much larger than, say, visible wavelengths, the manufacturing of radio antennas does not require the same skills as that of telescope mirrors and such antennas can reach very large sizes, implying an excellent sensitivity to faint signals. Gigantic base line interference arrays have been constructed, up to a size commensurate with the Earth diameter, allowing for very high resolutions. As a result, radio astronomy has contributed major data to nearly all branches of modern astrophysics, in particular pulsars, AGN and quasars and supernova remnants.

Yet, normal main sequence stars, such as our Sun, are very faint radio emitters and the radio sky does not show the stars which have been observed for several millennia by the naked eye and, more recently, by powerful telescopes. There is however an exception, a single exception, to this statement, which is precisely our Sun. The Sun is so close to the Earth that, in spite of its very faint radio emission, it still is the strongest radio source in our sky, stronger than the Crab (a pulsar), stronger than Sgr A (the black hole at the centre of the Milky Way), stronger than Cen A (the closest AGN, at the centre of two colliding galaxies) and stronger than all SNRs. It can be observed with relatively modest instruments and such an observation is the subject of the present thesis.

In 1995, a solar eclipse occurred in South Viet Nam, in the province of Phan Thiet. On that occasion Pr Nguyen Quang Rieu, an astronomer at the Meudon Observatory, near Paris, brought there a small radio interferometer that had been built by radio astronomers in Nançay (France) [1] and observed the decline, extinction and revival of the solar signal [2]. The interferometer was left in Vietnam as a gift in the hope that it could be of help for introducing modern astrophysics to Vietnamese students. Unfortunately, there being no teaching of modern astrophysics in Vietnam, it had been left dormant for nearly fifteen years. The work presented here reports on the refurbishing of this instrument and on observations of the Sun that have been made using it.

The first four parts of the thesis introduce the subject with overviews of the physics of the Sun (Part 1), of the mechanisms of radio emission from space (Part 2), of present day's radio astronomy (Part 3) and of the main features of the radio Sun (Part 4). The fifth part describes the apparatus, the preparatory measurements that have been made with it and the principle of the method. The last part reports on the observations made and on the analysis of the data. The thesis closes with a very brief summary and considerations on possible perspectives for the future.

# 1. THE SUN: GENERAL FEATURES

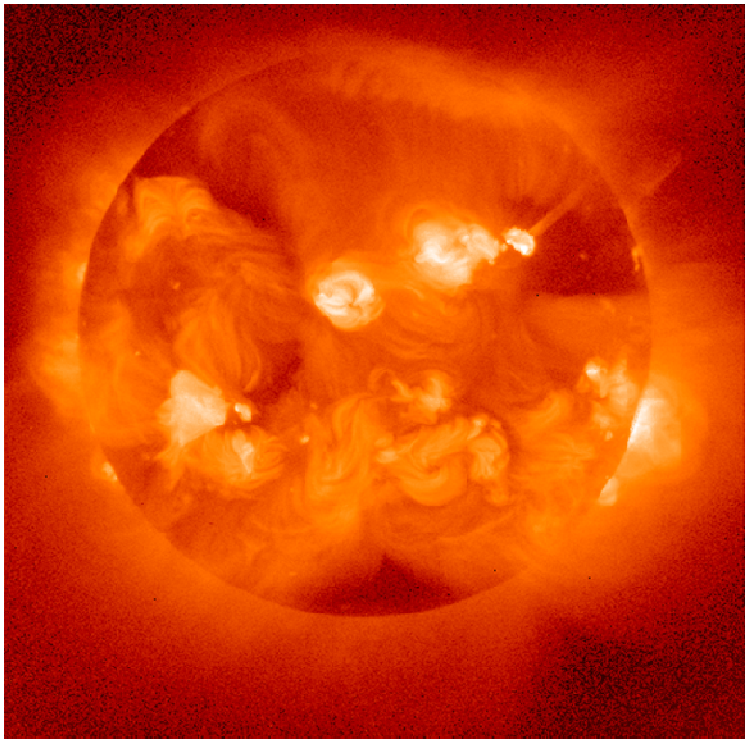

Figure 1.1. The Sun as seen in X-ray.

The Sun, the star at the centre of the Solar System, was born some 5 billion years ago from the gravitational collapse of a molecular cloud. It is located 1 astronomical unit (AU, 8.3 light minutes) away from the Earth. It is a main sequence star with a surface temperature of ~5.8 kK. Its energy supports almost all life on Earth via photosynthesis and drives its climate and weather.

The Sun generates its energy by nuclear fusion of hydrogen nuclei into helium. There are some $10^{11}$ stars of its type in the Milky Way. It consists of hydrogen (~ 74% in mass), helium (~ 24% in mass), and traces of other elements. Its spectrum contains lines of ionized and neutral metals as well as very weak hydrogen lines. The Sun's hot corona continuously expands in space creating the solar wind, a hypersonic stream of charged particles that extends to some 100 AU. It orbits the centre of the Milky Way at a distance of approximately 25,000 light years from the galactic centre, moving at a speed of 250 km/s in the direction of Cygnus and completing one revolution in nearly 250 million years. The Sun will keep burning its hydrogen into helium for another 5 billion years, after which it will become a red giant and ultimately die as a white dwarf, leaving a planetary nebula on the way.

## 1.1 Structure of the Sun

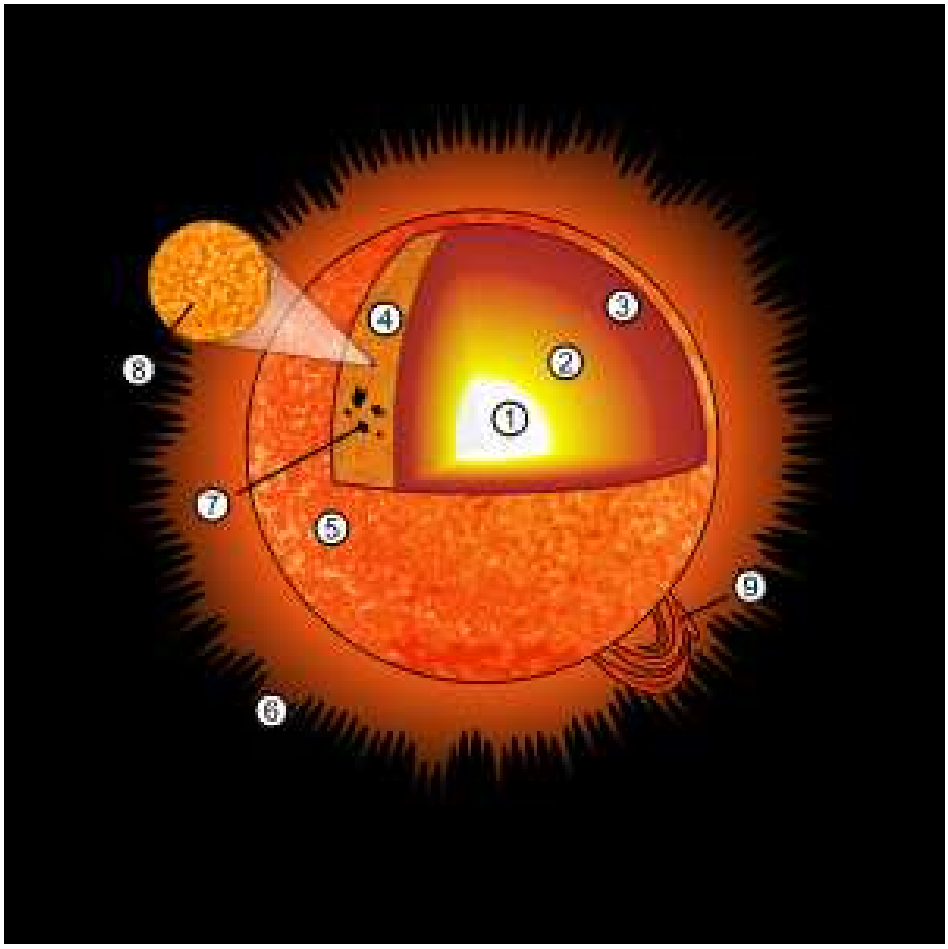


Figure 1.2. Schematic illustration of the structure of the Sun:1. Core; 2. Radiative zone; 3. Convective zone; 4. Photosphere; 5. Chromosphere; 6. Corona; 7. Sunspot; 8. Granules; 9. Prominence.

The Sun is a yellow main sequence star accounting for about 99.86% of the total mass of the Solar System. It is a nearly perfect sphere (Figure 1.1). As the Sun is not a solid but a plasma, it rotates faster at its equator than at its poles. This behaviour is known as differential rotation. The period of this actual rotation is approximately 25.6 days at the equator and 33.5 days at the poles. Accounting for our constantly changing vantage point from the Earth as it orbits the Sun, the apparent rotation of the star at its equator is about 28 days.

The Sun is a Population I, or heavy element-rich, star. The formation of the Sun may have been triggered by shockwaves from one or more nearby supernovae. This is

suggested by a high abundance of heavy elements in the Solar System, such as gold and uranium, relative to the abundances of these elements in so-called Population II (heavy element-poor) stars.

The Sun does not have a definite boundary, and in its outer parts the density of its gases drops approximately exponentially with increasing distance from its centre. Nevertheless, it has a well-defined interior structure (Figures 1.2 and 1.3), described below. The Sun's radius is measured from its centre to the edge of the photosphere. This is simply the layer above which the gases are too cool or too thin to radiate a significant amount of light, and is therefore the surface most readily visible to the naked eye.

The solar interior is not directly observable, and the Sun itself is opaque to electromagnetic radiation. However, just as seismology uses waves generated by earthquakes to reveal the interior structure of the Earth, helioseismology makes use of pressure waves (infrasound) traversing the Sun's interior to measure and visualize the star's inner structure. Computer modelling of the Sun is also used as a theoretical tool to investigate its deeper layers.

### *1.1.1 Core*

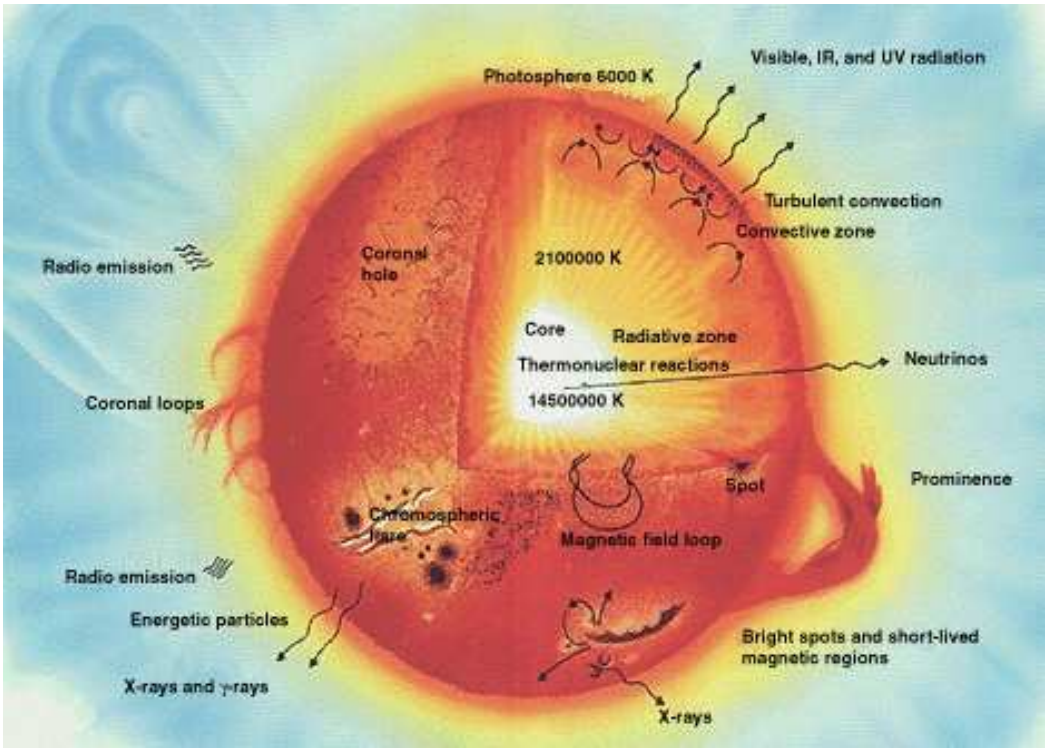


Figure 1.3. Schematic cross-section of a solar-type star

The core of the Sun is considered to extend from the centre to about 0.2 to 0.25 solar radii. It has a density of up to 150 g/cm$^3$ and a temperature of 13.6 MK (by contrast, the surface of the Sun is around 5.8 kK). Through most of the Sun's life, energy is produced by nuclear fusion through a series of steps called the p–p cycle[1]; this process converts hydrogen into helium. Less than 2% of the helium generated in the Sun comes from the CNO cycle. The core is the only location in the Sun that produces an appreciable amount of heat via fusion: the rest of the star is heated by energy that is transferred outward from the core. All of the energy produced by fusion in the core must travel through many successive layers to the solar photosphere before it escapes into space as sunlight or kinetic energy of particles.

About $10^{38}$ protons (out of ~$10^{57}$) are converted into helium nuclei every second. Power density is about 0.2 mW/kg of matter; but since most fusion occurs in the relatively small core the plasma power density in the core is about 150 times bigger. For comparison, the human body produces heat at the approximate rate of 1.3 W/kg, roughly 600 times greater per unit mass. Assuming a core density 150 times higher than average, this corresponds to a surprisingly low rate of energy production in the Sun's core—about 0.27 W/m$^3$. This power is much less than generated by a single candle. The rate of nuclear fusion depends strongly on density and temperature, so the fusion rate in the core is in a self-correcting equilibrium: a slightly higher rate of fusion would cause the core to heat up and expand slightly against the weight of the outer layers, reducing the fusion rate and correcting the perturbation; and a slightly lower rate would cause the core to cool and shrink slightly, increasing the fusion rate and again reverting it to its original level.

The high-energy photons released in fusion reactions are absorbed in only a few millimetres of solar plasma and then re-emitted again in random direction (at slightly lower energy) – so it takes a long time for radiation to reach the Sun's surface. Estimates of the "photon travel time" (an improper name, it is not the same photon that travels!) range between 10 and 170 kyr.

After a final journey through the convective outer layer to the transparent "surface" of the photosphere, the photons escape as visible light. Each gamma ray in the Sun's core ends up generating several million visible light photons escaping into space. Neutrinos are also released by the fusion reactions in the core, but unlike photons they rarely interact with matter, so almost all are able to escape the Sun immediately.

### *1.1.2 Radiative zone*

[1] The pp cycle is p p –> d e ν, d p –> $^3$He γ, $^3$He $^3$He –> $^4$He p p and the CNO cycle p $^{12}$C –> $^{13}$N γ, $^{13}$N –> $^{13}$C e ν, $^{13}$C p –> $^{14}$N γ, $^{14}$N p –> $^{15}$O γ, $^{15}$O –> $^{15}$N e ν, $^{15}$N p –> $^{12}$C $^4$He γ , namely 4p –> $^4$He + 2eν + 2γ for pp and 4p –> $^4$He + 2eν + 4γ for CNO.

From ~0.25 to ~0.7 solar radii, solar material is hot and dense enough for thermal radiation to transfer the intense heat of the core outward. In this zone there is no thermal convection; while the material grows cooler as altitude increases (from 7 MK to about 2 MK) this temperature gradient is too low to drive convection. Heat is transferred by photons emitted by excited hydrogen and helium atoms, which travel only a brief distance before being reabsorbed. The density drops a hundredfold (from 20 g/cm$^3$ to only 0.2 g/cm$^3$) from the innermost to outermost part of the radiative zone.

Between the radiative zone and the convection zone is a transition layer called the tachocline. This is a region where the sharp regime change between the uniform rotation of the radiative zone and the differential rotation of the convection zone results in a large shear – a condition where successive shells slide past one another. The fluid motions found in the convective zone slowly disappear when moving inwards to match the calm characteristics of the radiative zone. It is commonly accepted that a magnetic dynamo within this layer generates the Sun's magnetic field.

### *1.1.3 Convective zone*

In the Sun's outer layer, from its surface down to approximately 70% of the solar radius, the solar plasma is not dense enough or hot enough to transfer the heat energy of the interior outward by radiation. As a result, thermal convection occurs as thermal columns carry hot material to the surface (photosphere) of the Sun. Once the material cools off at the surface, it plunges back downward to the base of the convection zone, to receive more heat from the top of the radiative zone. At the visible surface of the Sun, the temperature has dropped to 5.7 kK and the density to only 0.2 g/m$^3$.

The thermal columns in the convection zone form an imprint on the surface of the Sun, in the form of the solar granulation. The turbulent convection of this outer part of the solar interior gives rise to a “small-scale” dynamo that produces magnetic north and south poles all over the surface of the Sun.

### *1.1.4 Photosphere*

The effective temperature, or black body temperature of the Sun, 5777 K, is the temperature that a black body of the same size must have to yield the same total emissive power (Figure 1.4).

The visible surface of the Sun, the photosphere, is the layer below which the Sun becomes opaque to visible light. Above the photosphere visible sunlight is free to propagate into space, and its energy escapes the Sun entirely. The change in opacity is due to the decreasing amount of $H^-$ ions, which absorb visible light easily. Conversely, the visible light we see is produced as electrons react with hydrogen atoms to produce

$H^-$ ions. The photosphere is actually tens to hundreds of kilometres thick, being slightly less opaque than air on Earth. Because the upper part of the photosphere is cooler than the lower part, an image of the Sun appears brighter in the centre than on the edge or *limb* of the solar disk, in a phenomenon known as limb darkening. Sunlight has approximately a black-body spectrum (~ 6 kK) interspersed with atomic absorption lines from the tenuous layers above the photosphere. The photosphere has a particle density of ~$10^{23}$ $m^{-3}$, ~1% of the particle density of Earth's atmosphere at sea level.

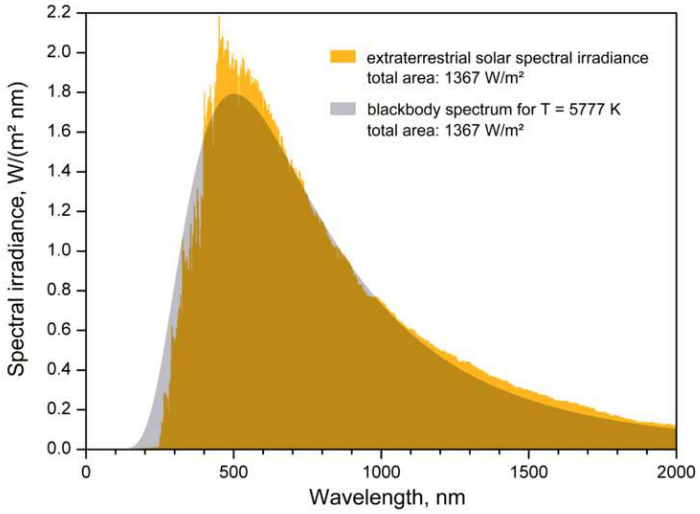


Figure 1.4. Comparison of the solar extraterrestrial spectrum with a black body spectrum.

### *1.1.5 Atmosphere*

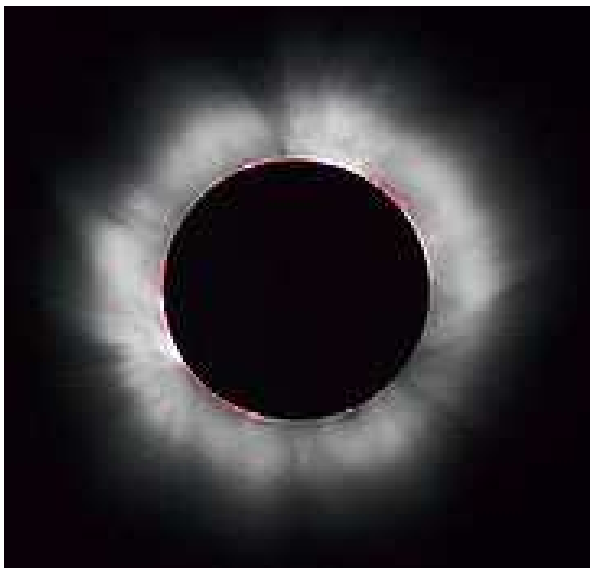

Figure 1.5. The solar corona as seen on the occasion of a total solar eclipse. During a total solar eclipse, the solar corona can be seen with the naked eye.

The parts of the Sun above the photosphere are referred to collectively as the *solar atmosphere*. They can be viewed with telescopes operating across the electromagnetic spectrum, from radio through visible light to gamma rays, and comprise five principal zones: the *temperature minimum*, the chromosphere, the transition region, the corona, and the heliosphere. The heliosphere, which may be considered as the tenuous outer atmosphere of the Sun, extends outward past the orbit of Pluto to the heliopause, where it forms a sharp shock front boundary with the interstellar medium. The chromosphere, transition region, and corona are much hotter than the surface of the Sun. The reason why has not been conclusively elucidated but there exist some evidence in favour of plasma waves (Alfvén waves) having sufficient energy to heat the corona.

The coolest layer of the Sun is a temperature minimum region about 500 km above the photosphere, with a temperature of about 4 kK. This part of the Sun is cool enough to support simple molecules such as carbon monoxide and water, which can be detected by their absorption spectra.

Above the temperature minimum layer is a layer about 2’000 km thick, dominated by a spectrum of emission and absorption lines. It is called the *chromosphere* from the Greek *chroma*, meaning colour, because the chromosphere is visible as a coloured flash at the beginning and end of total eclipses of the Sun. The temperature in the chromosphere increases gradually with altitude, ranging up to around 20 kK near the top. In the upper part of the chromosphere helium becomes partially ionized.

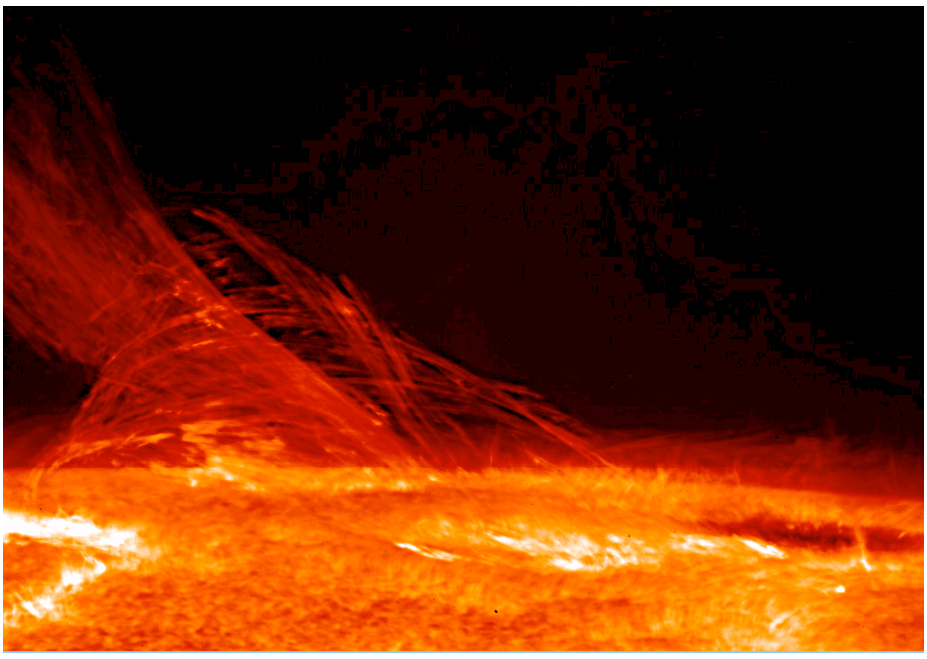

Figure 1.6. Taken by Hinode’s Solar Optical Telescope on January 12, 2007, this image of the Sun reveals the filamentary nature of the plasma connecting regions of different magnetic polarity.

Above the chromosphere there is a thin (about 200 km) transition region in which the temperature rises rapidly from around 20 kK in the upper chromosphere to coronal temperatures closer to 1 MK. The temperature increase is eased by the full ionization of helium in the transition region, which significantly reduces radiative cooling of the plasma. The transition region does not occur at a well-defined altitude. Rather, it forms a kind of halo around chromospheric features such as spicules and filaments, and is in constant, chaotic motion. The transition region is not easily visible from Earth's surface, but is observable from space by instruments sensitive to the extreme ultraviolet portion of the spectrum.

The corona (Figure 1.5) is the extended outer atmosphere of the Sun, which is much larger in volume than the Sun itself. The corona continuously expands into space forming the solar wind, which fills the whole Solar System. The low corona, very near the surface of the Sun, has a particle density around $10^{15}$ to $10^{16}$ $m^{-3}$. The average temperature of the corona and solar wind is about 1 to 2 MK, reaching 8 to 20 MK in the hottest regions. While no complete theory yet exists to account for the temperature of the corona, some of its heat is known to be from magnetic reconnection (Figure 1.6).

The heliosphere, which is the cavity around the Sun filled with the solar wind plasma, extends from approximately 20 solar radii (0.1 AU) to the outer fringes of the Solar System. Its inner boundary is defined as the layer in which the flow of the solar wind becomes *superalfvénic* — that is, where the flow becomes faster than the speed of Alfvén waves. Turbulence and dynamic forces outside this boundary cannot affect the shape of the solar corona within it, because the information can only travel at the speed of Alfvén waves. The solar wind travels outward continuously through the heliosphere, forming the solar magnetic field into a spiral shape (Figure 1.7), until it impacts the heliopause more than 50 AU from the Sun.

## 1.2 Magnetic field

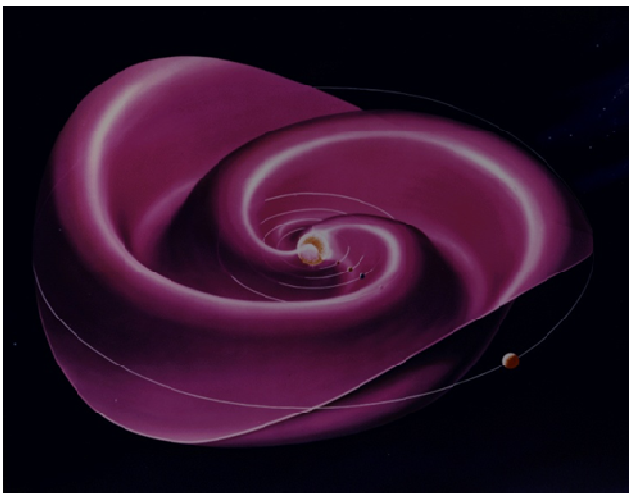

Figure 1.7. Structure of the Sun magnetic field

The heliospheric current sheet extends to the outer reaches of the Solar System, and results from the influence of the Sun's rotating magnetic field on the plasma in the interplanetary medium.

### *1.2.1 General features*

The Sun is a magnetically active star. It supports a strong, changing magnetic field that varies year-to-year and reverses direction about every eleven years around solar maximum. The Sun's magnetic field gives rise to many effects that are collectively called solar activity, including sunspots on the surface of the Sun, solar flares, and variations in solar wind that carry material through the Solar System. Effects of solar activity on Earth include auroras at moderate to high latitudes, and disturbance of radio communications and electric power distribution. Solar activity is thought to have played a large role in the formation and evolution of the Solar System. Solar activity changes the structure of Earth's outer atmosphere.

The differential rotation of the Sun's latitudes causes its magnetic field lines to become twisted together over time, causing magnetic field loops to erupt from the Sun's surface and trigger the formation of the Sun's dramatic sunspots and solar prominences. This twisting action gives rise to the solar dynamo and an 11-year solar cycle of magnetic activity as the Sun's magnetic field reverses itself about every 11 years.

### *1.2.2 Interplanetary field*

The solar magnetic field extends well beyond the Sun itself. The magnetized solar wind plasma carries Sun's magnetic field into the space forming what is called the interplanetary magnetic field. Since the plasma can only move along the magnetic field lines, the interplanetary magnetic field is initially stretched radially away from the Sun. Because the fields above and below the solar equator have different polarities pointing towards and away from the Sun, there exists a thin current layer in the solar equatorial plane, which is called the heliospheric current sheet. At large distances the rotation of the Sun twists the magnetic field and the current sheet into an Archimedean spiral-like structure called the Parker spiral (Figure 1.7). The interplanetary magnetic field is much stronger than the dipole component of the solar magnetic field. The Sun's 50–400 μT (in the photosphere) magnetic dipole field reduces with the cube of the distance to about 0.1 nT at the distance of the Earth. However, according to spacecraft observations the interplanetary field at the Earth's location is about 100 times greater, around 5 nT.

The embedment of the Earth magnetic field in that of the Sun gives rise to the Earth magnetosphere, which has a complex structure. In particular magnetic bottles

near the Earth poles trap particles from the solar wind, giving rise to spectacular auroras (Figure 1.8).


Figure 1.8. The magnetic field structure in the neighbourhood of the Earth (left) and a photograph of an aurora (right).

### *1.2.3 Sunspots and solar cycle*

When observing the Sun with appropriate filters, the most immediately visible features are usually its sunspots, which are well-defined surface areas that appear darker than their surroundings because of lower temperatures. Sunspots are regions of intense magnetic activity where convection is inhibited by strong magnetic fields, reducing energy transport from the hot interior to the surface. The magnetic field gives rise to strong heating in the corona, forming active regions that are the source of intense solar flares and coronal mass ejections. The largest sunspots can be tens of thousands of kilometres across.

The number of sunspots visible on the Sun is not constant, but varies over the 11-year solar cycle (Figures 1.9 and 1.10). At a typical solar minimum, few sunspots are visible, and occasionally none at all can be seen. Those that do appear are at high solar latitudes. As the sunspot cycle progresses, the number of sunspots increases and they move closer to the equator of the Sun, a phenomenon described by Spörer's law. Sunspots usually exist as pairs with opposite magnetic polarity. The magnetic polarity of the leading sunspot alternates every solar cycle, so that it will be a north magnetic pole in one solar cycle and a south magnetic pole in the next.

### *1.2.4 Anomalies*

The solar cycle, while having a negligible influence on solar irradiance on Earth, has a significant influence on its climate via magnetic activity. A higher

magnetic activity prevents more cosmic rays to reach the Earth and to contribute to cloud formation, hence implying a lesser cloud coverage and global warming: solar activity minima tend to be correlated with colder temperatures, and longer than average solar cycles tend to be correlated with hotter temperatures. In the 17th century, the solar cycle appears to have stopped entirely for several decades. Very few sunspots were observed during that period, which is known as the Maunder minimum or Little Ice Age, and Europe experienced very cold temperatures. Earlier extended minima have been discovered through analysis of tree rings and also appear to have coincided with lower-than-average global temperatures.

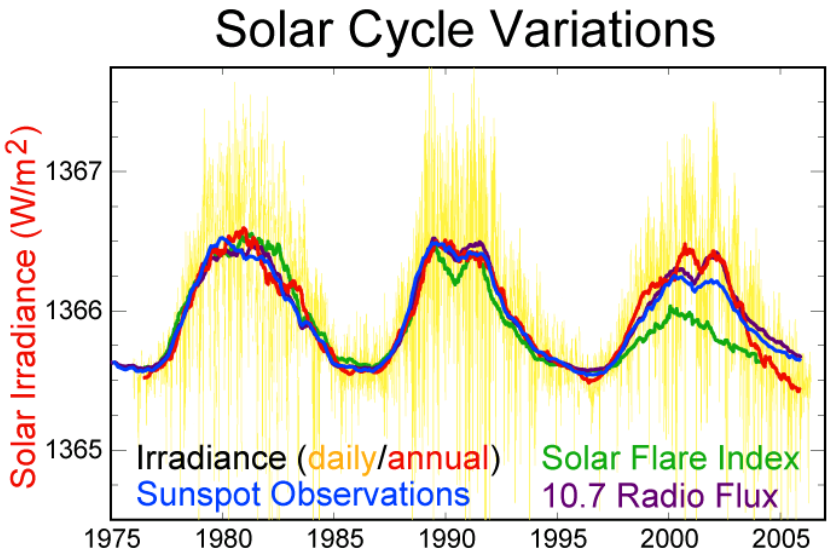


Figure 1.9. Measurements of solar cycle variation during the last 30 years

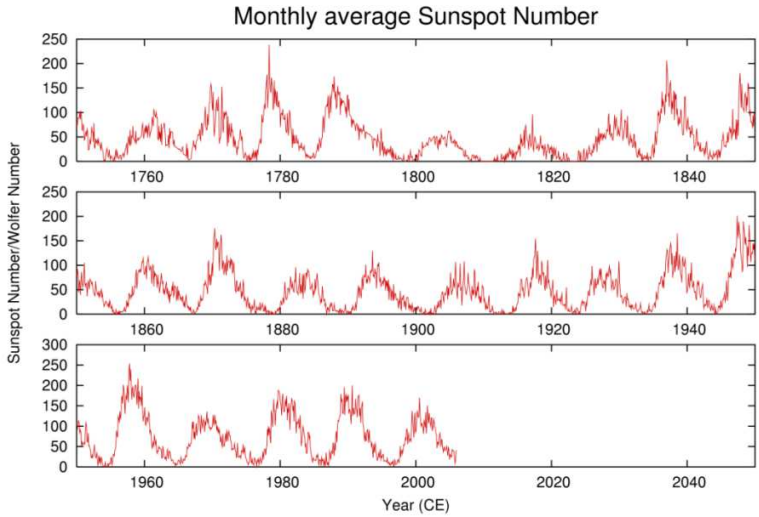


Figure 1.10. History of the number of observed sunspots during the last 250 years, showing the ~11-year solar cycle.

The Sun is presently behaving unexpectedly in a number of ways. While its wind has steadily increased over the XXth century, it is now in the midst of an unusual sunspot minimum, lasting longer and with a higher percentage of spotless days than normal; since May 2008, predictions of an imminent rise in activity have been regularly made and as regularly confuted. It is measurably dimmer than is usual during a sunspot minimum. Over the last two decades, the solar wind's speed has dropped by 3%, its temperature by 13%, and its density by 20%. Its magnetic field is at less than half strength compared to the minimum of 22 years ago. The entire heliosphere, which fills the Solar System, has shrunk as a result, resulting in an increase in the level of cosmic radiation striking the Earth and its atmosphere.

## 1.3 Evolution

### *1.3.1 Birth of the Sun*

The Sun was formed about 5 billion years ago when a hydrogen molecular cloud collapsed. Solar formation is dated in two ways: the Sun's current main sequence age, determined using computer models of stellar evolution and nucleocosmochronology, is thought to be about 4.57 billion years. This is in close agreement with the radiometric date of the oldest Solar System material.

The Sun is composed primarily of hydrogen and helium; they account respectively for 74.9% and 23.8% of its mass in the photosphere. All heavier elements, called *metals* in astronomy, account for less than 2 percent of the mass. The most abundant metals are oxygen (roughly 1% of the Sun's mass), carbon (0.3%), neon (0.2%) and iron (0.2%).

The Sun inherited its chemical composition from the interstellar medium out of which it was formed: the hydrogen and helium in the Sun were produced by Big Bang nucleosynthesis. The metals were produced by stellar nucleosynthesis in generations of stars which completed their stellar evolution and returned their material to the interstellar medium prior to the formation of the Sun. The chemical composition of the photosphere is normally considered representative of the composition of the primordial Solar System. However, since the Sun formed, the helium and heavy elements have settled out of the photosphere. Therefore, the photosphere now contains slightly less helium and only 84% of the heavy elements than the protostellar Sun did; the protostellar Sun was 71.1% hydrogen, 27.4% helium, and 1.5% metals.

### *1.3.2 Present status*

Theoretical models of the Sun's development suggest that 3.8 to 2.5 billion years ago, the Sun was only about 75% as bright as it is today. Such a weak star would not have been able to sustain liquid water on the Earth's surface, and thus life should not

have been able to develop. However, the geological record demonstrates that the Earth has remained at a fairly constant temperature throughout its history, and in fact that the young Earth was somewhat warmer than it is today. It is commonly accepted that the young Earth's atmosphere contained much larger quantities of greenhouse gases (such as carbon dioxide, methane and/or ammonia) than are present today, which trapped enough heat to compensate for the lesser amount of solar energy reaching the planet.

The Sun is about halfway through its main-sequence evolution (Figure 1.11), during which nuclear fusion reactions in its core fuse hydrogen into helium. Each second, more than 4 million tonnes of matter are converted into energy within the Sun's core, producing neutrinos and solar radiation; at this rate, the Sun will have so far converted around 100 Earth-masses of matter into energy. The Sun will spend a total of approximately 10 billion years as a main sequence star.

In the inner portions of the Sun, nuclear fusion has modified the composition by converting hydrogen into helium, so the innermost portion of the Sun is now roughly 60% helium, with the metal abundance unchanged. Because the interior of the Sun is radiative, not convective, none of the fusion products from the core have risen to the photosphere.

The solar heavy-element abundances described above are typically measured both using spectroscopy of the Sun's photosphere and by measuring abundances in meteorites that have never been heated to melting temperatures. These meteorites are thought to retain the composition of the protostellar Sun and thus not affected by settling of heavy elements. The two methods generally agree well.

### *1.3.3 Death of the Sun*

The Sun does not have enough mass to explode as a supernova. Instead, in about 5 billion years, it will enter a red giant phase; its outer layers will expand as the hydrogen fuel in the core is consumed and the core contracts and heats up. Helium fusion will begin when the core temperature reaches around 100 MK and will produce carbon, entering the asymptotic giant branch phase.

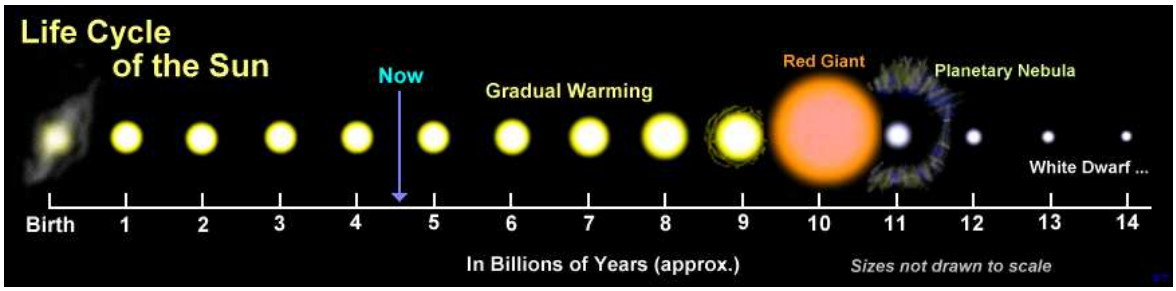


Figure 1.11. Life-cycle of the Sun; sizes are not drawn to scale.

Following the red giant phase, intense thermal pulsations will cause the Sun to throw off its outer layers, forming a planetary nebula. The only object that will remain after the outer layers are ejected is the extremely hot stellar core, which will slowly cool and fade as a white dwarf over many billions of years. This stellar evolution scenario is typical of low- to medium-mass stars.

# 2. RADIO EMISSION

## 2.1 Thermal Emission

Thermal emission is a basic form of emission of electromagnetic radiation. Any object having a temperature above absolute zero emits thermal radiation. The temperature of the object is a measure of the kinetic energy of the atoms and molecules which it is made of. Their movement implies constant changes of direction: the molecules of a gas, as in a planet's atmosphere, keep spinning around and bumping into one another. A change in direction is equivalent to acceleration. When charged particles accelerate, they emit electromagnetic radiation. So each time a molecule changes direction, it emits radiation across the spectrum.

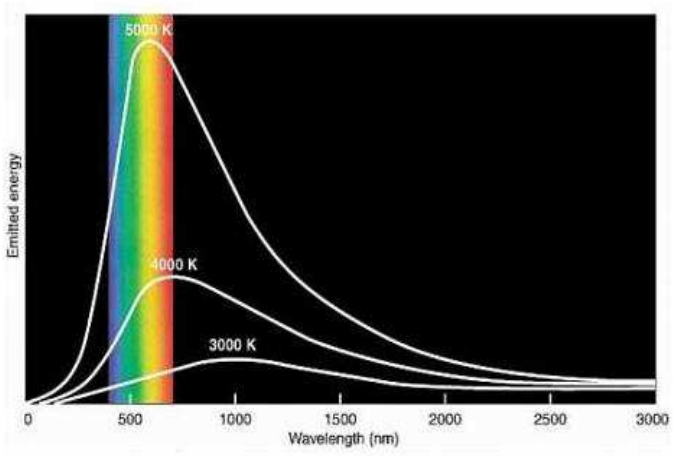


Figure 2.1. Black body spectra at three different temperatures. The visible region is indicated.

This is called blackbody radiation. A blackbody is, by definition, in thermal equilibrium: it completely absorbs all of the radiation that hits it, with no diffusion nor reflection, and radiates energy with a characteristic spectrum. The dependence upon wave length $\lambda$ of the power $P$ radiated per unit area peaks at a wavelength that depends only on the temperature $T$ and is given by Planck's law: $dP/d\lambda=2hc^2\lambda^{-5}/(exp[hc/kT\lambda]-1)$. Taking the derivative with respect to $\lambda$ gives Wien's laws: $\lambda_{max}\approx 2900\ \mu m.K/T$ and $T^{-5}dP/d\lambda\approx 8\pi\ \mu Wm^{-3}K^{-5}$ at maximum emission. Integrating instead over $\lambda$ gives $T^{-4}P=5.7\ 10^{-12}\ Wcm^{-2}\ K^{-4}$, the Stefan-Boltzmann law. Figure 2.1 shows blackbody spectra for objects at three different temperatures: 5 kK, 4 kK, and 3 kK. It is apparent from the image that objects at lower temperatures emit more radiation at longer wavelengths. Objects that are cooler than about 1 kK emit more infrared than visible light, such as the Earth or brown dwarfs (dim, cool objects too massive to be planets

but not massive enough to be stars). Hotter objects, like stars, emit mostly optical light. Very hot objects emit mostly ultraviolet radiation, such as white dwarfs (dying stars that have burned up all of the hydrogen in their cores). The Sun and other stars behave as blackbody radiators. By looking at the frequency or "colour" of the radiation they emit, one learns about their surface temperature. Cooler stars appear red and hotter stars appear bluish-white.

In order for an object to emit thermal radiation at radio wavelengths, it must be much colder than these objects. In the radio range, one is dealing with large wavelengths, far away on the right of Figure 2.1. One may then retain the first order term in $1/\lambda$ in the development of Planck's law which becomes the Rayleigh Jeans relation, $dP=2hc^2\lambda^{-5}d\lambda/(hc/kT\lambda) =2kTdv/\lambda^2$,where we have introduced the frequency $v=c/\lambda$. This relation of proportionality between temperature and power is very important in radio astronomy.

## 2.2 Free-Free (bremsstrahlung) emission

Another form of thermal emission comes from gas which has been ionized. This results in charged particles moving around in a plasma. As this happens, the electrons are accelerated by the ions, and the gas cloud emits radiation continuously. This type of radiation is called "free-free" emission (because the charged particle is free both before and after the emission of the bremsstrahlung photon) or bremsstrahlung. The energy radiated is inversely proportional to the square of the mass of the charged particle: hence most of bremsstrahlung radiation is emitted by electrons rather than by ions. The bremsstrahlung photons are emitted forward in a narrow cone and have a continuous energy spectrum of the form $1/E$.

## 2.3 Spectral lines

Spectral line emission involves the transition of electrons in atoms from a higher energy level to lower energy level. When this happens, a photon is emitted with the same energy as the energy difference between the two levels. The emission of this photon at a certain discrete energy shows up as a discrete line or wavelength in the electromagnetic spectrum.

An important spectral line that radio astronomers study is the 21cm line of neutral hydrogen. This line is emitted by the following transition: the hydrogen atom consists of one electron orbiting one proton. Both the electron and the proton have spin 1/2. In the lowest energy state, or ground state, the spins of both particles are in opposite directions. When the atom becomes excited, either by absorbing a photon, or by bumping into other atoms, the electron absorbs a small amount of energy, and the spin of the electron may flip so that the spins of both particles are in the same direction. When the atom reverts back to its natural state, it loses this energy by

emitting a photon with a wavelength of 21 cm, in the radio region of the electromagnetic spectrum.

Very remote galaxies have a high redshift: in such cases, spectral lines may be shifted to the radio range making radio astronomy a particularly valuable tool for the study of the far away Universe.

### 2.4 Synchrotron (non-thermal) emission

Non-thermal emission does not have the characteristic spectrum of blackbody radiation. In fact, it is quite the opposite, with emission increasing at longer wavelengths. The most common form of non-thermal emission found in astrophysics is called synchrotron emission. Basically, synchrotron emission arises by the acceleration of charged particles within a magnetic field. Most commonly, the charged particles are electrons. Compared to protons, they have a much smaller mass and are much easier to accelerate. The mechanism is precisely the same as for bremsstrahlung but the acceleration is now caused by magnetic field bending rather than by interaction with the Coulomb field of an atom.

In a magnetic field, electrons spiral around the field lines and continuously change their direction, thereby emitting radiation with a frequency directly related to the electron velocity and to the field strength. When an electron (charge $e$ and mass $m$) moves in a magnetic field $H$ at a velocity $\beta$ with respect to the light velocity, it follows an helix and emits synchrotron radiation, namely photons having a so-called Larmor frequency $f=eH/\{2m\sqrt{(1-\beta^2)}\}$ The maximum of the synchrotron emission is at a frequency $f(MHz)=0.5\ 10^{-3}E(eV)^2H(T)$. As the electron travels around the magnetic field, it looses energy as it emits photons. To maintain synchrotron emission, a continuous supply of relativistic electrons is therefore necessary. Typically, these are supplied by very powerful energy sources such as supernova remnants, quasars, or other forms of active galactic nuclei (AGN).

It is important to note that, unlike thermal emission, synchrotron emission is polarized.

### 2.5 Pulsars

A special form of synchrotron emission, known as gyro synchrotron emission, is emitted by pulsars. Pulsars result from the death of massive stars (stars with about 8 to 15 times the mass of the Sun). As a massive star runs out of nuclear fuel, its core begins to collapse. When the outer layers of the star collapse onto the core, a shock wave is produced that results in a massive explosion called a supernova, the core going from atomic densities to nuclear densities: one is left with a compact neutron star in the centre of a rapidly expanding supernova remnant (SNR). The neutron star measures a few kilometres in diameter and has a mass of at least 1.4 solar masses. As the core of the star collapses to vastly increased density, the magnetic field of the star is

accordingly amplified, magnetic flux being conserved, and so is its rotation frequency, angular momentum being conserved. The magnetic field is trapped in the outer shell of the neutron star, which is iron and nickel rich. Such a rapidly rotating neutron star is known as a pulsar**.** A typical pulsar has a magnetic field a trillion times stronger than the Earth's, which accelerates electrons and other subatomic particles to nearly the speed of light, causing them to emit beams of radiation, including radio waves. When these beams sweep across the Earth, we see a “pulse” of radiation from the pulsar. As the pulsar rotates, the radiation appears to flash on and off, similar to a lighthouse. Some pulsars rotate relatively slowly, such as the Crab (M1) which rotates 33 times per second. Other pulsars, known as millisecond pulsars**,** can rotate hundreds of times per second.

### 2.6 Masers

Another form of non-thermal emission comes from masers. A maser, which stands for “microwave amplification by stimulated emission of radiation”, is similar to a laser (which amplifies radiation at or near visible wavelengths). Masers are usually associated with molecules and, in space, masers occur naturally in molecular clouds and in the envelopes of old star. Maser action amplifies otherwise faint emission lines at a specific frequency. In some cases the luminosity from a given source in a single maser line can equal the entire energy output of the Sun from its whole spectrum.

# 3. RADIO ASTRONOMY: AN INTRODUCTION

## 3.1 An overview

Radio waves are the electromagnetic waves that have the longest wavelength, from 1 mm to 100 m. Above 100 m they are reflected by the ionosphere and cannot reach the Earth. In space, beyond the ionosphere, one could in principle (for example on the moon) detect radio waves up to 10 km wave length. Many astronomical objects emit radio waves. The first radio astronomical observations were made in 1932 by Karl Jansky, a Bell Lab physicist who detected cosmic radio noise from the Milky Way while investigating radio disturbances interfering with transoceanic communications. Since then, astronomers have built many radio telescopes with sophisticated systems

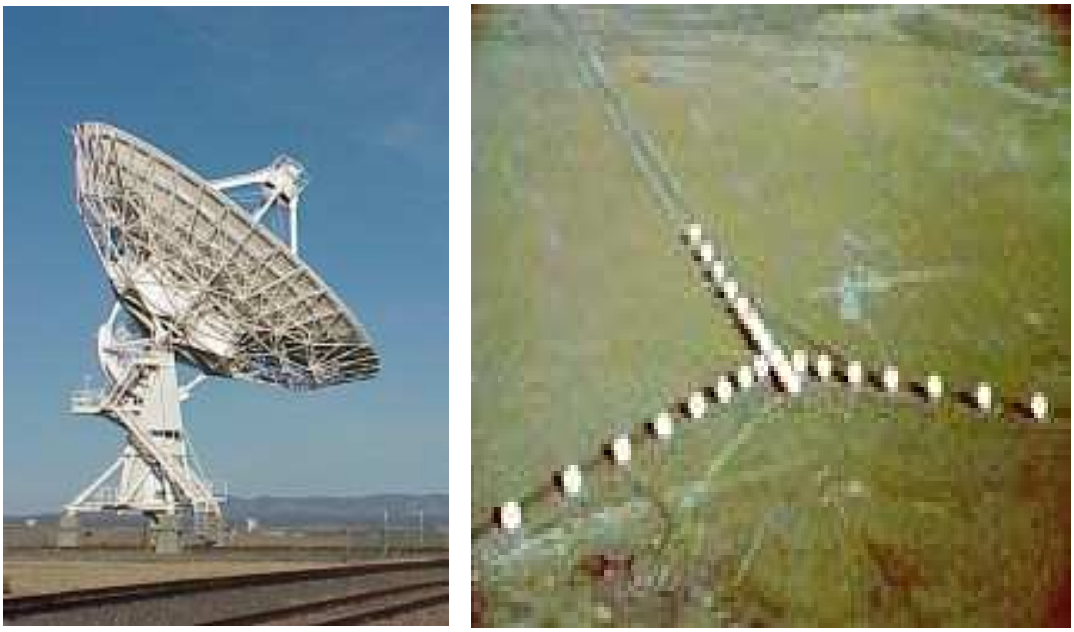

Figure 3.1: An antenna of the VLA (left) and the VLA array (right).

that allow for a high angular resolution resulting in the production of detailed radio pictures of celestial objects.

Radio telescopes have two basic components: a large radio antenna (or set of antennas) and sensitive radio receivers. As an example, the Very Large Array (VLA) is one of the world's best astronomical radio observatories (Figure 3.1). It consists of three equal arms of 9 antennas each, symmetrically arranged at $120^{o}$ from each other. The antennas are parabolic, 25 m in diameter and the array is up to 36 km across.

Incoming signals are collected by the dish of the antenna and reflected by its

parabolic surface to the focus called the “knobby widget” where there is either another reflector (as in the VLA) or a receiver. In the VLA the focal reflector is movable and can, at will (according to wave length), send the signal back to one of several waveguide terminals located in the centre of the dish. From there it is transferred to the receivers that are located below the antenna and cooled down to 15 K in order to minimize thermal noise. The receiver amplifies separately the two opposite circular polarizations components of the signal.

Differential fluxes (also called flux densities, i.e. fluxes per unit of frequency) are measured in Jansky ($10^{-26}$Wm$^{-2}$Hz$^{-1}$). When the flux has its source in thermal emission, the frequency spectrum is that of a black body with a Planck distribution. In the case of radio waves, where one is dealing with large wave lengths, the Planck relation reduces to the so-called Rayleigh-Jeans relation: the flux $\Phi$ is related to the black body temperature $T$ through the relation $\Phi=2kT/\lambda^2$ where $k$ is Boltzmann's constant and $\lambda$ the wave length. The lowest temperature that can be detected is limited by the detector thermal noise and is equal to $T_{min}=T_r/\sqrt{B\tau}$ where $B$ is the bandwidth, $\tau$ the time of integration and $T_r$ the temperature of the receiver. The lowest detectable flux is therefore $2kT_{min}/\lambda^2$. In practice, one can go down to $T_{min}=10$ K.

The sensitivity of a radio telescope, the ability to measure weak sources of radio emission, is proportional to the area and efficiency of the antenna and the sensitivity of the radio receiver used to amplify and detect the signal. For broadband continuum emission the sensitivity also trivially depends on the bandwidth of the receiver.

The angular resolution, or ability of a radio telescope to distinguish two neighbour sources, namely fine details in the sky, is limited by diffraction: it is equal to the ratio between the wavelength of observation and the diameter of the antenna of the instrument. This is at variance with ground observation in the visible where atmospheric turbulences (changing the index of refraction) rather than diffraction limit the angular resolution. For a same angular resolution a short wave length antenna will therefore afford to be smaller than a large wavelength antenna.

Radio waves penetrate much of the gas and dust in space as well as the clouds of planetary atmospheres and pass through the terrestrial atmosphere with little distortion. In principle, radio astronomers can therefore obtain a much clearer picture of stars and galaxies than is possible by means of optical observation from ground. However this requires the use of very large antennas.

The first large parabolic antenna was built in Jodrell Bank (United Kingdom) in 1957 (Figure 3.2). It has a diameter of 75 m and detects wave lengths larger than 15 cm. The largest movable parabolic antenna ever built is 100 m in diameter and is located in the Eiffel Mountain (Germany) near Bonn. In1963 Cornell University built a fixed antenna in Arecibo (Porto Rico). It is 305 m in diameter and is installed in a natural basin (Figure 3.3). It is made of a metallic grid resting on cables and the receiver, hanging 150 m above ground, can move around by $\pm 20^o$.

Building significantly larger antennas is not possible: thermal deformations and,

more importantly, mechanical deformations in the case of a movable antenna, distort the shape of the detector beyond the permissible limit, i.e. a fraction of a wave length – typically one tenth.

Figure 3.2 The Jodrell Bank antenna in the United Kingdom is 75 m in diameter.

Figure 3.3. Aerial view of the Arecibo antenna in Porto Rico

However, interferometry allows for much better angular resolutions: having two antennas far apart is the same as having two small distant pieces of a very large antenna as far as angular resolution is concerned (but of course, as far as sensitivity is concerned, it is not: the only way to increase the sensitivity is to increase the size of the receptor or to lower $T_{min}$). This is the idea of interferometry which implies that the two antennas, distant from each other, are positioned to better than a fraction of a wavelength (as they should be if they were part of a same reflector). In practice this is done by looking at the interference pattern between the two receivers. Such arrays of antennas have been built in several sites around the world and the VLA is the best such example. One can even, in principle, have antennas separated by as much as an Earth diameter. Indeed networks of such antennas exist and the data are recorded together with the time given by an atomic clock and are combined later on in a computer.

As mentioned earlier, radio sources can produce radio waves by thermal emission (usually resulting from the thermal movement of electrons and ions in a plasma) or by non thermal emission (such as synchrotron radiation or coherent movements in oscillating plasmas).

Thermal emission obeys the Rayleigh Jeans relation. Planets have their maximum of emission in the infrared. Interesting information is obtained from a comparison of their temperatures measured with radio waves or with infrared radiations. For example Venus is found to be at 600K by radio and at 225 K by infrared. The reason is the clouds that surround it and the green house effect that results. Radio waves probe the surface of the planet while infrared radiation probes the clouds. In situ measurements have confirmed these results. Outside of the solar system radio waves are good detectors of gas clouds in the interstellar matter, of supernova remnants and of plasmas of various kinds.

In addition to these continuous spectra there are also line spectra in radio astronomy as there are in the visible. The most famous is the 21cm hydrogen line (corresponding to the spin-flip of the electron of a neutral atom). But there also exist many other molecular lines that tell us which molecules are present in interstellar clouds. Moreover, line spectra allow for a measurement of the velocity of the object from their Doppler shift. One should also mention that measuring the polarization of radio waves provides useful additional information.

Figure 3.4 below shows an overall view of the radio sky in galactic coordinates with a clear contribution of the Milky Way, in particular near the galactic centre, and of active galaxies, such as Cen A (above the equator, a bit on the right).

## 3.2 Radio instruments

### *3.2.1 Antennas*

The elements of a standard radio telescope are the reflector, feed, transmission

line and receiver. The reflector collects power from an astronomical source and provides directionality. The terms antenna and reflector are often used interchangeably.

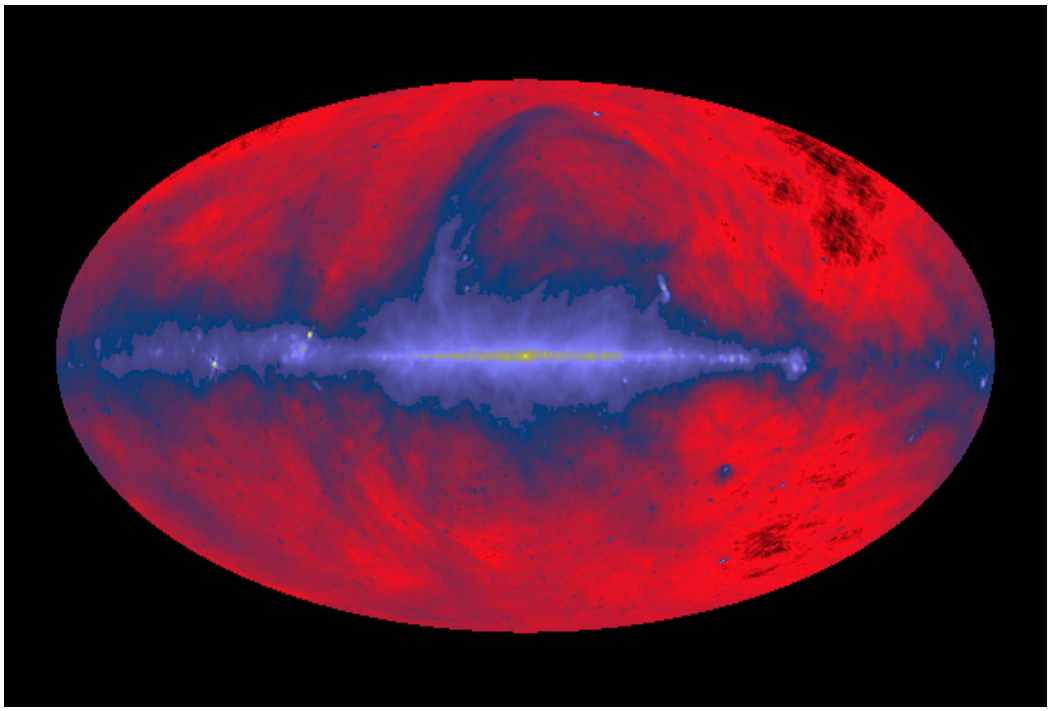

Figure 3.4. The radio sky 408 MHz continuum image *(Haslam et al. 1982, A &AS, 47, 1)* (galactic coordinates)

However, there is a difference: an antenna is a device that couples the waves in free space to the confined waves in a transmission line while reflectors concentrate the radiation. The reflector or antenna has two purposes, first it collects power and second it provides directionality. The power collected by an antenna is approximately given by $P=S_\nu A\ \Delta\nu$ where $S_\nu$ is the flux density on Earth from some astronomical source, $A$ is the effective area of the antenna and $\Delta\nu$ is the frequency interval or bandwidth of the measured radiation. So, the larger antennas collect more power. The antenna also has the capability of discriminating the signals coming from different directions in space.

An important and useful theorem, the reciprocity theorem, states that an antenna operates the same way whether it is receiving or transmitting radiation. So the response pattern of an antenna that is receiving radiation is the same as the pattern produced when the same antenna is transmitting.

A telescope's response pattern is then the same as the far-field diffraction pattern produced by the aperture. In general, when radiation of wavelength $\lambda$ passes through an aperture of diameter $D$, the radiation diffracts into a beam with angular size $\theta = \lambda /D$. At large distances (or the far-field response), the pattern is given by Fraunhofer diffraction theory and the pattern looks like that in Figure 3.5, where the beam width is

the full width at half power of the main beam. The beam width $\theta$ is also a measure of the directivity of the antenna. A more precise statement that can be made is that the angular pattern of the electric field in the far-field is the Fourier transform of the electric field distribution across the aperture.

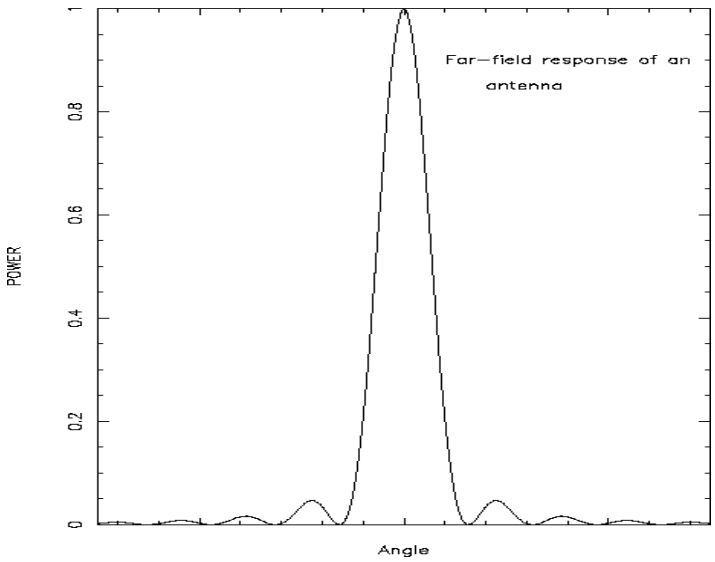


Figure 3.5. Fraunhofer pattern of a typical antenna response.

Radio and radar engineers normally speak about antennas in terms of their gain in dB referred to a half-wave dipole (dBd) or referred to an ideal isotropic antenna (dBi). We recall that 20 dB corresponds to a factor 10 in amplitude and the number of dB is proportional to the decimal logarithm of the amplitude[2]. A half-wave dipole has a gain of 2.15 dBi. Radio astronomers prefer to talk of size and efficiency or effective collecting area. The gain, *G*, of an antenna relative to isotropic is related to its effective collecting area, *A*, by $G = 4\pi A/\lambda^2$ where $\lambda$ is the wavelength. This means that the power collected in the pointing direction by an effective area *A* is *G* times higher than what an ideal isotropic antenna would collect, namely $\lambda^2/4\pi$. The beam solid angle is $\Omega_A=4\pi/G$ corresponding to a cone of $arctan(2/\sqrt{G})$ half aperture (measured in radians).

The gain is therefore related to the directivity of the antenna: an antenna with a smaller beam will have a higher gain. If we think of the antenna as a transmitter, as we can do owing to reciprocity, then if the transmitted energy is confined to a narrow angle, the power in this direction must be higher than average in order for the total power radiated in all directions to add up to the total power transmitted.

To achieve an effective area or aperture of many square wavelengths (gains of

[2] In radio, and generally at RF frequencies, the gain is calculated as the ratio of powers *P* (and not amplitudes *A* as we are used to). One usually calls gain, evaluated in dB, $10\ log_{10}(P_{out}/P_{in})=20\ log_{10}(A_{out}/A_{in})$. A factor 2 is 3 dB (+ for amplification and – for attenuation), a factor 10 is 10 dB.

more than, say, 26 dBd), a parabolic reflector is the simplest and best approach. For long wavelengths, for which an antenna with more than 26 dBd would have enormous dimensions, other approaches are more appropriate. As radio amateurs doing Moon-bounce know, it is hard to beat an array of Yagi antennas for simplicity and minimum wind loading. A single 20-wavelength-long Yagi can give a gain of 20 dBd. Stacking 2 Yagi's adds 3 dB and another 3 dB for every doubling. The effective aperture of a 20 dBd Yagi, however, is only 13 square wavelengths, so that stacking 50 Yagi's to get 37 dBd of gain at, say, 4 GHz doesn't make much sense when one can do as well with a 9-foot-diameter dish of 60% efficiency. At UHF frequencies around 400 MHz, the choice between Yagi's and a dish is not so clear.

With the availability of excellent Low Noise Amplifiers (LNAs), optimizing the antenna efficiency is less important than optimizing the ratio of efficiency to system noise temperature or gain over system temperature, *G/Ts*. This means that using a feed with low side lobes and slightly under-illuminating the dish may reduce *Ts* by more than it reduces *G* and so improve sensitivity.

With the advent of excellent LNAs, the antenna noise is also a very important performance parameter along with the gain or equivalent effective aperture. Antenna noise originates from the sky background, Ohmic losses, and ground pickup or *spill over* from side lobes. While the sky noise is fundamental, the losses and side lobes can be made small by a good design. Sky noise is frequency dependent but never gets any lower than the cosmic 3-K background. The minimum is near 1.4 GHz, where Galactic noise has declined and atmospheric attenuation, due primarily to the water line at 22 GHz, is still low. The lowest system noise achievable is about 18 K. At the NASA deep space network (DSN) the S-band (2.3 GHz) system budget is approximately 3 K from cosmic background plus 7 K spill over plus 3 K atmospheric plus 5 K LNA. At 408 MHz, galactic noise will dominate, and system noise will be at least 50 K increasing to over 100 K toward the Galactic centre.

### *3.2.2 Receivers*

Radio telescope receivers filter and detect radio emission from astronomical sources. In most cases the emission is incoherent radiation whose statistical properties do not differ either from the noise originating in the receiver or from the background radiation that is coupled to the receiver by the antenna. In addition, these signals are extremely weak, so amplifiers have to be constructed in order to increase the signal to a detectable level.

After the antenna, the first stage of the receiver, the low-noise amplifier (LNA), is probably the most important component of a radio telescope. Since the signals are so weak, the noise performance of the receiver is crucial, and this leads to extraordinary efforts, such as cryogenic cooling, to reduce noise in the LNA. The noise performance of radio-astronomy receivers is usually characterized by an equivalent system

temperature, $T_{sys}$, referred to the feed or even to outside Earth's atmosphere. Using temperature units for the system allows direct comparison with source temperatures. Typical system temperatures are ten to a hundred K for centimetre wavelengths or up to several hundred K for millimetre and sub-millimetre wavelengths.

Most receivers used in radio astronomy (all receivers used for spectroscopy) employ so-called super heterodyne schemes. The goal is to transform the frequency of the signal (SF) down to a lower frequency, called the intermediate frequency (IF) that is easier to process but without losing any of the information to be measured. This is accomplished by mixing the SF from the LNA with a local oscillator (LO) and filtering out any unwanted sidebands in the IF. A bonus is that the SF can be shifted around in the IF, or alternatively, the IF for a given SF can be shifted around by shifting the LO.

Inside radio-astronomy receivers, a signal is usually represented by a voltage proportional to the electric field (as collected by the antenna). As it averages to zero, one needs a device that produces an output proportional to the square of the voltage, a so-called square-law detector, and that averages over at least a few cycles of the waveform. This is achieved naturally in the case of non linear response where the non linearity is quadratic to first order. We return to this argument in Section 5.

### *3.2.3 Extracting weak signals from noise*

As mentioned above, radio-astronomy systems usually operate close to the theoretical noise limits. With a few exceptions, signals are usually extremely weak. One such exception is the Sun. Depending on frequency, solar cycle, antenna size and system noise temperature, pointing an antenna at the Sun normally increases the received power several fold. Toward other sources, it is not unusual to detect and measure signals that are less than 0.1% of the system noise. The increase in power, measured in K, due to the presence of a radio source in the beam is given by $2kT_a=AF$ where $A$ is the effective aperture (or aperture efficiency times physical aperture), $F$ is the radio flux density in watts/m$^2$/Hz, and $k$ is Boltzmann's constant, 1.38 x 10$^{-23}$ W/Hz/K. While voltages in the antenna add up linearly at a given time, the lack of coherence between signal and background (unrelated phases) implies that they must be added in quadrature (i.e. the square root of the sum of their squares) to obtain the summed voltage averaged over several RF periods: it is indeed power that is relevant.

The factor of 2 in the left hand side of the above relation is because radio astronomers usually define the flux density as that present in both wave polarizations, but a receiver is sensitive to only one polarization. Radio telescopes use linear or circular polarization depending on the type of observations being made, and with two LNAs and two receivers, one can detect two orthogonal polarizations simultaneously. In order to detect and measure signals that are a very small fraction of the power passing through the receiver, signal averaging or *integration* is used. If the receiver gain is perfectly stable, our ability to measure small changes in signal is proportional to

the square root of the time of integration.

If the receiver bandwidth is 1 MHz and the system temperature is $T_{sys}$=100 K, for example, then we can measure down to 0.013 K in one minute. For a sure detection, one needs to see a change of $10\ \sigma$ or about 0.1 K change. The receiver gain in practice is seldom exactly constant, and the additional spill over noise and atmospheric noise may also be changing, so it will be difficult at this level to distinguish a real signal from a change in gain or atmospheric noise. There are several solutions to this problem, depending on the type of observation, all of which rely on some way of forming a reference. If one is making spectral-line measurements, the reference is often just adjacent frequencies. If one scans the frequency or simultaneously divide the spectrum into many frequency channels, then the gain or atmospheric noise changes will be largely common to all frequencies and will cancel with baseline subtraction in the final spectrum. In making measurements of broadband or *continuum* radio emission, one may use a synchronous detection technique known as *Dicke* switching: one uses of a switch to toggle the input of the LNA between two antenna outputs that provide adjacent beams in the sky. If one switches fast enough in this case and take the difference between the powers of the two outputs synchronously with the antenna switch, then receiver gain changes will largely cancel. Furthermore, if the two antenna beams are close together on the sky, then changes in the atmospheric noise will tend to be common to both beams and will also cancel. Since one is taking a difference and spending half the time looking at the reference, the actual observation time is halved.

Another powerful technique for extracting weak signals from noise is correlation. The radio telescope in this case has two or more receivers either connected to the same antenna, or, more often, two or more separate antennas. The signal voltages are multiplied together before averaging instead of multiplying the signal voltage by itself to obtain the power. With separated antennas, the correlation output combines the antenna patterns as an interferometer, which generates lobes on the sky that are separated in angle by the wavelength divided by the projected baseline between the antennas.

### *3.2.4 Analogue-to-digital converter (ADC)*

Since all the final processing of a radio telescope output is done with a computer, one needs to convert analogue voltages from the detector to numbers that can be processed in software. A very accurate and effective ADC is a voltage-to-frequency converter followed by a counter. This ADC provides integrated power with as many bits as are needed to represent the count over the integration interval. If reading the output of the counter at perfectly regular intervals is difficult, then another counter can be used simultaneously to count the constant-frequency output of a crystal oscillator. The integrated power is then proportional to the ratio of the counts from the

voltage-to-frequency converter to the counts from the crystal oscillator.

### *3.2.5 Interference*

Radio astronomy is often limited by interference especially at low frequencies. The spectrum is overcrowded with transmitters: Earth-based TV, satellite TV, FM, cellular phones, radars, and many others. Radio astronomy has some protected frequency bands, but these bands are often contaminated by harmonics accidentally radiated by TV transmitters, intermodulation from poorly designed transmitters, and noise from leaky high-voltage insulators and automobile ignition noise. Some of the worst offenders are poorly designed satellite transmitters, whose signals come from the sky so that they affect even radio telescopes that are well shielded by the local terrain. Radio telescopes and their receivers can be made more immune to interference by:

– Including a band pass filter following the LNA to prevent interference from being generated inside the receiver by intermodulation.

– Placing the telescope in a location with as much shielding as possible from the local terrain. Low spots (e.g., valleys) are good for low-frequency radio telescopes because they reduce the level of interference from ground-based transmitters.

– Tracking down interference and trying to reduce it at the source.

– Designing and using an antenna with very low side lobes.

– Using an interferometer and correlation processing: this is far more immune to interference.

– Using data editing to remove data corrupted by interference.

# 4. THE RADIO SUN

The study of solar radio waves was launched in earnest in the post-war years, when many physicists the world over salvaged surplus radar equipment whose antennas and receivers were ideal for studying the Sun. Today the radio Sun has been observed across the radio spectrum and modern solar radio astronomy is rich of details which cannot be mentioned here where we present only some of the highlights. The Sun emits radio signals through the synchrotron radiation process, which involves high-speed electrons spiralling around magnetic fields, as well as thermal radiation from the hot plasma, which is produced by virtue of the motion of the electrons in the plasma. A third mechanism, which has many variations, involves natural oscillations of the plasma itself: radio emission can occur at the frequency of the plasma oscillations as well as multiples of this frequency.

## 4.1 The quiet Sun

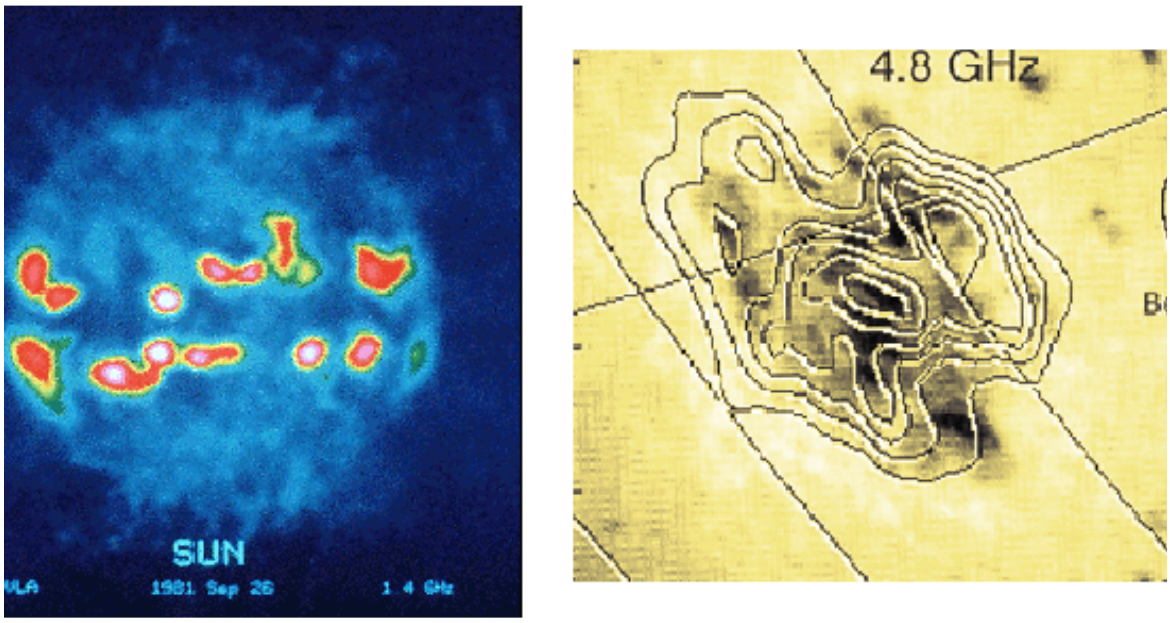


Figure 4.1: *Left:* The 20 cm radio Sun observed with the VLA during the magnetic activity maximum on September 26, 1981. The patches of enhanced emission are predominantly due to optically thick free-free emission from coronal plasma. (Copyright by the Smithsonian Institution). *Right:* Radio emission (contours) from above a sunspot group (grey scale plot), observed at 6 cm (4.8 GHz) with the Owens Valley Radio Observatory. Much of the emission is due to optically thick gyro resonance emission in concentrated (~1 kG) magnetic fields. (Gary & Hurford 1994; courtesy of D. Gary.)

Radio emission from the quiet sun is observed at times of sunspot minimum and comes from regions low in the corona. A slowly varying component may be observed which varies with the rotation of the Sun, one cycle after every 28 days. The variable intensity is partly related to the presence of cooler regions known as coronal holes, which alternate with a slightly warmer, more normal plasma, over the solar surface.

The quiet Sun, by definition, is observed when there is little violent activity occurring. The slowly varying component is partly related to the presence of filaments of hotter gas, which thread their way over the solar disk. In their immediate neighbourhood, temperatures change from 6 kK in the filaments to 2 MK in the surrounding corona, which has long been known to be extraordinarily hot for reasons that remain unclear.

The non-flaring Sun has been studied at metre, decimetre and centimetre wavelengths in appreciable detail. Fig. 4.1 (left) shows the Sun observed near its activity maximum with the Very Large Array (VLA) at 20 cm wavelength. Figure 4.1 (right) illustrates a close-up view of 6 cm radio emission (contours) in the vicinity of a sunspot group. The emission contributions vary strongly during the magnetic activity cycle; at maximum, most of the measured flux stems from active regions. The dominant emission mechanism depends on the observing frequency and on the source location with respect to active region magnetic field structures. The type of dominant emission can be derived in particular from the spectral behaviour on the optically thin side of the spectrum. Roughly speaking, the longer-wavelength emission (e.g. at 20 cm Fig. 4.1) is dominated by optically thick coronal free-free emission that correlates well with soft-X-ray features (identical emission mechanism). At a wavelength of 6 cm, active region emission consists of bright compact sources and a diffuse halo. The halo component is often due to optically thin thermal free-free emission from the corona, but also from the cooler transition region and the chromosphere.

Both types of emission can be used effectively to derive principal source parameters, namely the electron temperature from either of the optically thick emissions, the electron density from the bremsstrahlung components, and the magnetic field strengths from the gyro resonance emission. Strong magnetic fields up to 2 kG can be present even at coronal levels. Such values are close to photospheric levels; they indicate that the magnetic field divergence from the photosphere to coronal layers is rather small.

## 4.2 Flares

On a regular basis, especially when many sunspots are present, regions on the surface of the Sun may grow steadily hotter and brighter until a flare explosion occurs. Near such active regions, whether or not accompanied by a flare activity, bursts of radio waves may be generated (Figure 4.2) whose variations in frequency and over

time can be very complex.

During flares, the Sun can be a source of copious radio *gyro synchrotron* emission for up to tens of minutes. The emission is produced by accelerated, mildly relativistic electrons spiralling around the magnetic field lines. This radiation often reaches its peak flux in the 1 to 10 GHz region. Its spectrum contains rich diagnostic information: electron energies can be derived from the optically thick portion, magnetic field strengths from the turnover frequency, and the electron energy distribution from the optically thin part.

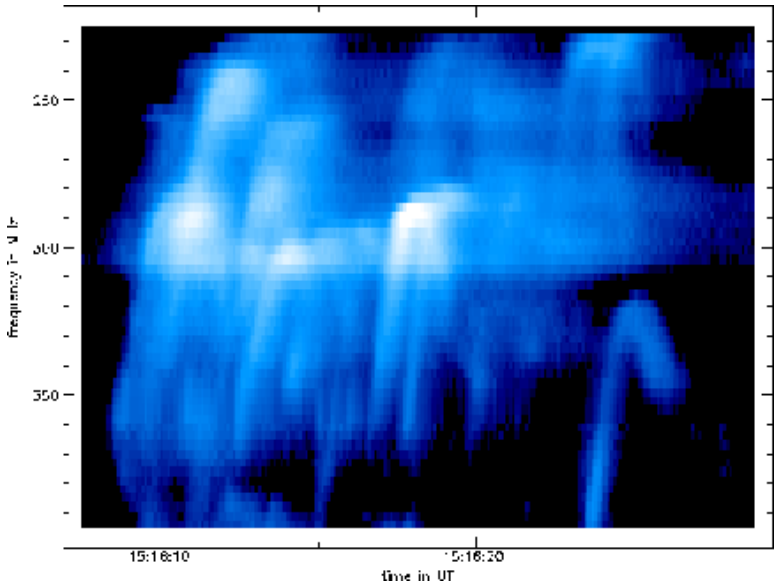


Figure 4.2: Extract from a dynamic spectrum of a solar type U radio burst group (9 July 1980). U bursts are generated by the beam plasma instability. The emission at the plasma frequency traces closed coronal loops. (From the RAG data archive, Institute of Astronomy, ETH Zürich.)

# 5. THE VATLY SOLAR INTERFEROMETER: DESCRIPTION AND SETTING-UP

## 5.1 Principle of the method

Consider two antennas $A_1$ and $A_2$ separated by a distance $L=|\boldsymbol{A_1A_2}|$ (baseline) and oriented in the Sun direction defined by unit vector $\boldsymbol{u}$ (Figure 5.1). The radio signal emitted by the Sun covers a very broad frequency domain and the antennas collect whatever fraction of it falls within their bandwidth centred on frequency $f$. As a function of time $t$, the output voltage in antenna $A_i$ is $V_i= E_i sin(2\pi ft+\varphi_i)$. We take $\varphi_1= -\varphi_2= \frac{1}{2}\Delta\varphi$ by properly choosing the origin of time. The time delay between the signals received by the two antennas (the Sun is at infinity) corresponds to a phase difference $\Delta\varphi=2\pi f\tau$ where $\tau=\boldsymbol{A_1A_2}.\boldsymbol{u}/c$.

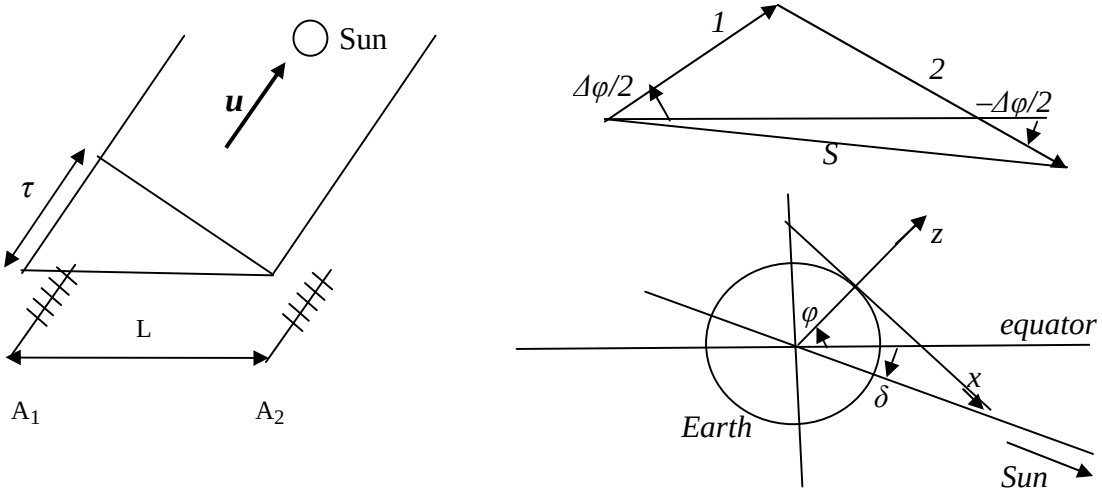


Figure 5.1. Left: the two-antennas interferometer. Right up: adding the signals in the complex plane. Right down: Noon geometry.

Adding both signals, and writing $S=exp(2i\pi ft)\{E_1 exp(2i\pi f\tau/2)+E_2\, exp(-2i\pi f\tau/2)\}$, the sum signal is the imaginary part of $S$. The first exponential oscillates very rapidly and averages to zero; its amplitude is the absolute value of the expression in the curly bracket which oscillates slowly with frequency $1/\tau$. It reads:
$S=|E_1 exp(2i\pi f\tau/2)+E_2 exp(-2i\pi f\tau/2)|=\{E_1^2+E_2^2+2E_1E_2 cos2\pi f\tau\}^{1/2}$. Writing the wave length $\lambda=c/f$ and the relative amplitude $r=E_2/E_1$, one may rewrite
$S= E_1\{1+r^2+2r cos(2\pi\boldsymbol{A_1A_2}.\boldsymbol{u}/\lambda)\}^{1/2}$.

In order to evaluate the scalar product, we take a local reference frame having the $x$ axis horizontal toward south, the $y$ axis horizontal toward east and the $z$ axis

vertical upward. As the base line is approximately east-west, we write $\boldsymbol{A_1A_2}=(\xi, -L+\eta, \zeta)$ where $\xi$, $\eta$, and $\zeta$ account for small deviations of the base line from its nominal value. The unit vector $\boldsymbol{u}$ is a function of the latitude $\varphi$ of the place of observation, the declination $\delta$ of the Sun and the hour angle $H$:

$\boldsymbol{u}=(-\cos\varphi\sin\delta+\sin\varphi\cos\delta\cos H, -\cos\delta\sin H, \sin\varphi\sin\delta+\cos\varphi\cos\delta\cos H)$.

At noon, when $H=0$, $\boldsymbol{u}=(\sin[\varphi-\delta], 0, \cos[\varphi-\delta])$.

Finally, the modulus of the added signal reads:

$S= E_1\{1+r^2+2r\cos(2\pi D/\lambda)\}^{½}$

with $D=\boldsymbol{A_1A_2}.\boldsymbol{u}$ (1)

$=\xi(-\cos\varphi\sin\delta+\sin\varphi\cos\delta\cos H)+(L-\eta)\cos\delta\sin H+\zeta(\sin\varphi\sin\delta+\cos\varphi\cos\delta\cos H)$.

For $r=1$ and $\xi=\eta=\zeta=0$, $S=\sqrt{2E_1\{1+\cos(2\pi D/\lambda)\}}^{½}=2E_1|\cos \pi D/\lambda|$ and $D=L\cos\delta\sin H$.

At equinox ($\delta=0$) around noon, in the approximation where $\lambda<<L$, the period of the interference is $T\sim\lambda/L$. In minutes, $T\sim(720/\pi)\lambda/L$; for $\lambda=50cm$ and $L=25m$, $T\sim(720/\pi)/50=4.6mn$.

The antennas have a lobe width such that the Sun stays within their range long enough to allow for the observation of several interference fringes without changing their orientation. Note that if the antennas are not perfectly pointing to the Sun, the interference term is unaffected: all what may change is the absolute intensity and the ratio $r$. In practice, the Sun emission will be superimposed on a background that depends on the environment, which must be chosen sufficiently quiet electromagnetically for the background to vary slowly, or better to remain constant during the measurement.

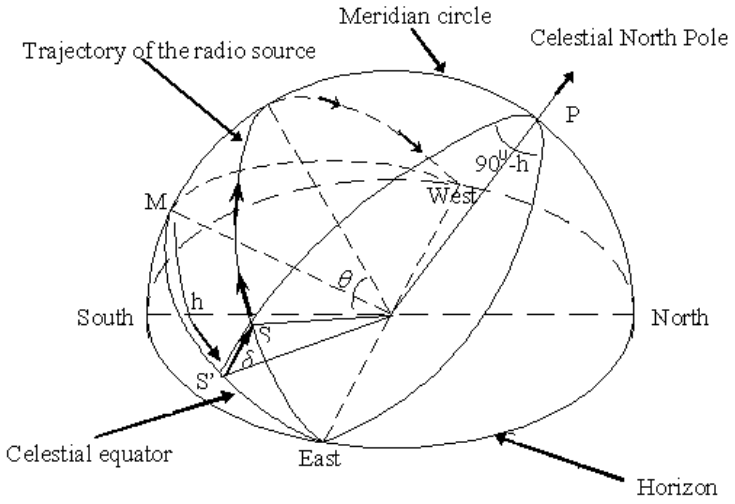


Figure 5.2. Coordinates relevant to the observation of a radio-source

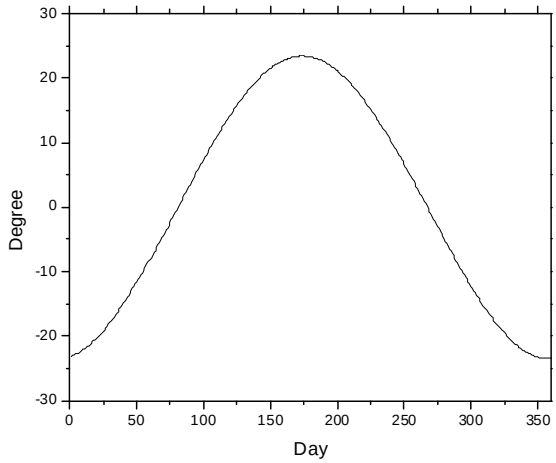


Figure 5.3. Dependence of the maximal declination of the Sun (at zero hour angle) as a function of date (starting from January 1st). The quantity of relevance is essentially the difference between the declination of the Sun and the latitude of Hanoi ($21^o$).

Part of the measurements has been made with a flagpole mount, the antennas being pointed toward the Sun visually. It was soon realized that this was not very convenient and simple equatorial mount stands have been constructed and used in the final measurements (Figure 5.4). They allow for a rotation of the antenna axis around a fixed axis pointing south downward by $21^o$, the Hanoi latitude. The angle between the antennas and the rotation axes needs only to be adjusted once in a while to follow the seasonal variation of the Sun declination.

Figure 5.4 Antenna mountings. Left: early flagpole mounting on the roof of our laboratory. Right: equatorial mounting in Hoa Binh. The arrows indicate the second antenna.

## 5.2 Signal detection and antennas

### *5.2.1 Power expected from the Sun and antenna temperature*

On Earth, we receive ~3 $10^{-21}$ W/m$^2$/Hz from the quiet Sun [3], equally shared between left and right polarization. While supposedly entering a new cycle of activity, the Sun is still today in a very quiet state [4]. Therefore with 0.6 MHz bandwidth and with 0.6 m$^2$ effective antenna area we receive some 0.5 $10^{-15}$ W (including the effect of polarization). The signal is amplified by some 80 dB to give some 50 nW at the detector input, meaning ~2 mV under 50 Ω at the input of the detector.

This signal level needs to be compared with the expected noise and interference levels. Some comes from TV emissions and other sources of electro-magnetic pollution and some is of thermal origin. It is convenient to introduce the concept of antenna temperature to discuss noise. An antenna temperature is associated with a given signal, namely a flux density $F$ emitted by some celestial object. The flux density is an energy per second of emission (or observation) per area of antenna and per Hertz: it is measured in $Wm^{-2}Hz^{-1}$ or in Jansky ($10^{-26}$ $Wm^{-2}Hz^{-1}$). Namely, in the case of a white noise or of a continuous spectrum (as is the case here for the Sun) the power collected within a bandwidth $\Delta\nu$ by an antenna of effective area $A$ is $P=\frac{1}{2}FA\Delta\nu$ where the factor ½ is due to the fact that the antenna accepts only one polarization state. The power received per Hz is therefore an energy, $\frac{1}{2}FA$, corresponding to a temperature $T_a=\frac{1}{2}FA/k$ where $k$ is Boltzmann constant, $1.38\ 10^{-23}$ $W/Hz/K$. In the case of a signal having a well defined frequency, the power received is independent of the bandwidth (the narrower the bandwidth, the better the signal to noise ratio) and the concept of antenna temperature is only useful when referred to noise. The temperature $T_a$ is called the antenna temperature for the particular signal under consideration. It may sound strange to have energy rather than power to define the level of the signal; this comes from the fact that a second of observation times a Hertz of band width is a pure number but the two factors entering this product are of a very different nature. According to Rayleigh Jeans relation, a black body of area $\lambda^2$ at temperature $T_a$ emitting isotropically emits a power per Hertz $2kT_aF$ which is precisely the flux density collected by the antenna.

When a same antenna receives white noise signals from different sources, the electric fields induced in it by each of these sources add up at any given time. In particular, for two signals $E_1$ and $E_2$, the antenna sees a field $\{ E_1^2+E_2^2+2E_1E_2\cos\Delta\varphi \}^{\frac{1}{2}}$ where the phase difference $\Delta\varphi$ has a flat distribution when the two signals are unrelated: on average, the cosine term cancels and the antenna behaves as detecting power rather than voltage, as it really does. The amplitude $E$ of the detected sine wave is the square root of the sum of the squares of the amplitudes of the sine waves induced by each signal separately (one says that one adds them in quadrature). The detected signal being then transferred to the receptor via a line of impedance $R$, its power is $\frac{1}{2}E^2/R$ which is therefore the sum of the powers received by each white noise signal

separately. In the present case it is the sum of the power received from the Sun and of those received from various background sources. Hence the interest to use the concept of antenna temperature: the antenna temperature of the background and noise is the sum of the antenna temperatures of its various components and can be directly compared to the antenna temperature of the solar signal.

### *5.2.2 TV interference*

TV emissions cover part of the VHF band (Very High Frequencies) from 30 to 300 MHz and part of the UHF band (Ultra High Frequencies) from 300 MHz to 3 GHz. The VHF part is from 160 to 250 MHz and the UHF part is from 470 to 870 MHz.

We work in UHF, at a frequency around 600 MHz, because VHF frequencies are crowded by all kinds of other emissions. A list of the TV stations of relevance, including emission power $P_{TV}$, frequency $f_{TV}$ and distance to Hanoi $D_{TV}$ (in metres), is given in Table 5.1. Using this information we have estimated the power received in Hanoi by adding Gaussian contributions of the form:
$P_{TV}=(1/4\pi)(0.3/D^2)\exp\{-(f-f_{TV})^2/(2\sigma_{TV}^2)\}/(\sigma_{TV}\sqrt{2\pi})$ from each individual emitter (however using an effective antenna area of 0.3 $m^2$ instead of 0.6 $m^2$). The factor $(1/4\pi)(0.3/D^2)$ corresponds to the solid angle, relative to $4\pi$ at reception in the 0.3 $m^2$ antenna and the factor $(\sigma_{TV}\sqrt{2\pi})$ is the area under the Gaussian, $\sigma_{TV}$ being the rms value taken equal to 2.5 MHz. Figure 5.5 shows the result of this calculation, namely the frequency dependence of the received power per MHz. For a bandwidth of 0.6 MHz and an effective antenna area of 0.6 $m^2$, the power received by our antennas is therefore 20% larger. A minimum is reached at 611 MHz with a power of ~ 1.6 $10^{-10}$ W, namely some 5 orders of magnitude above the Sun signal. However, thanks to the directionality of the antenna, this factor will be significantly reduced. Table 5.2 lists the two Vietnamese TV stations emitting between 605 and 615 MHz together with the corresponding powers received in our detector. There must exist other TV stations at shorter distance to Hanoi outside Vietnam, in particular in China, Thailand, Laos and Cambodia. However, we did not collect information on these.

### *5.2.3 Antennas*

We use standard TV antennas (Yagi type) consisting of a folded dipole with reflecting bars behind and directing bars in front. Our antennas are for TV channels 31 to 49, meaning 550 to 750 MHz. They include the dipole, 2 reflecting bars and 9 directing bars. Yagi antennas have an approximate gain equal to 5/3 of the number of directing bars, namely ~15 dB, meaning that they are 30 times more sensitive in the direction in which they point than they would be if they were isotropic. This means that the power collected in the direction to which they point is the power collected by

an effective area $A$ which is $G=10^{1.5}=31.6$ times higher than what an ideal isotropic antenna would collect, namely $\lambda^2/4\pi=0.020\ m^2$. Their nominal effective area is therefore $A=0.63\ m^2$ and the beam solid angle is $\Omega_A=4\pi/G=0.40\ sr$ corresponding to a cone of 39° half aperture.

The antennas were first attached on flagpoles on the roof of the laboratory at a distance of 20 m from each other on an east-west base line. Later on they were installed on equatorial mounting supports (Figure 5.4). When pointing to large zenith angles, they were used in vertical polarization to minimize interferences from TV or other parasitic emissions.

Table 5.1. List of TV emitters with relevant parameters

| Location | Longitude | Latitude | Distance | Power | Chanel | Frequency | Power |
|---|---|---|---|---|---|---|---|
| | d m s | d m s | km | kW | | MHz | W |
| TX Vinh Phuc | 105E3741 | 21N1717 | 35.05681 | 5 | 41 | 634 | 6.48E-08 |
| TP Hai Duong | 106E1952 | 20N5607 | 54.80482 | 5 | 40 | 626 | 2.65E-08 |
| TX Tuyen Quang | 105E1255 | 21N4905 | 107.8183 | 5 | 34 | 578 | 6.85E-09 |
| TP Viet Tri | 105E2438 | 21N1914 | 53.14151 | 5 | 36 | 594 | 2.82E-08 |
| TX Bac Ninh | 106E0440 | 21N1130 | 33.32063 | 5 | 37 | 602 | 7.17E-08 |
| TX Hoa Binh | 105E2029 | 20N4901 | 54.02234 | 5 | 33 | 570 | 2.73E-08 |
| TP Ha Long | 107E0714 | 20N5830 | 135.9922 | 10<br>10 | 33<br>36 | 570<br>594 | 8.61E-09<br>8.61E-09 |
| TX Thai Binh | 106E2016 | 20N2649 | 84.29616 | 5 | 35 | 586 | 1.12E-08 |
| TP Nam Dinh | 106E1059 | 20N2610 | 75.89697 | 5 | 37 | 602 | 1.38E-08 |
| TX Ninh Binh | 105E5800 | 20N1400 | 89.36295 | 5 | 39 | 618 | 9.96E-09 |
| TP Da Nang | 108E1325 | 16N0343 | 607.6011 | 10 | 37 | 602 | 4.31E-10 |
| TX Tam Ky-QN | 108E2842 | 15N3526 | 671.6749 | 10 | 33 | 570 | 3.53E-10 |
| TX Quang Ngai | 108E4744 | 15N0719 | 728.2163 | 10<br>10 | 35<br>38 | 586<br>610 | 3.00E-10<br>3.00E-10 |
| TX Phan Thiet-BT | 108E0609 | 10N5526 | 1149.662 | 10 | 34 | 578 | 1.20E-10 |
| Phuoc Long-BP | 107E0001 | 11N4859 | 1031.882 | 10 | 35 | 586 | 1.49E-10 |
| TP Bien Hoa-DN | 106E5204 | 10N5707 | 1125.89 | 10 | 36 | 594 | 1.26E-10 |
| TX Ba Ria-BRVT | 107E1006 | 10N2939 | 1180.086 | 5 | 38 | 610 | 5.71E-11 |
| TP Vung Tau | 107E0437 | 10N2101 | 1194.831 | 5 | 41 | 634 | 5.57E-11 |
| TX Tan An-L An | 106E2431 | 10N3204 | 1168.411 | 10 | 34 | 578 | 1.17E-10 |
| TP Long Xuyen-AG<br>Nui Cam | 105E2518<br>104E5850 | 10N2346<br>10N2950 | 1182.793<br>1174.177 | 10<br>10 | 36<br>41 | 594<br>626 | 1.14E-10<br>1.15E-10 |
| TX Ben Tre | 106E2250 | 10N1418 | 1201.146 | 5<br>5 | 37<br>40 | 602<br>626 | 5.52E-11<br>5.52E-11 |
| TX Tra Vinh | 106E2047 | 09N5657 | 1233.095 | 5 | 35 | 586 | 5.23E-11 |
| TX Bac Lieu | 105E4123 | 09N1747 | 1304.441 | 10 | 33 | 570 | 9.35E-11 |
| TP Ca Mau | 105E0920 | 09N1109 | 1318.549 | 10 | 39 | 618 | 9.15E-11 |

Table 5.2. Vietnamese TV stations emitting in the frequency range of relevance

| Location | Longitude | Latitude | Distance | Power | Chanel | Frequency | Power |
|---|---|---|---|---|---|---|---|
| | d m s | d m s | km | kW | | MHz | W |
| TX Quang Ngai | 108E4744 | 15N0719 | 728.2163 | 10 | 38 | 610 | 3.00E-10 |
| TX Ba Ria-BRVT | 107E1006 | 10N2939 | 1180.086 | 5 | 38 | 610 | 5.71E-11 |

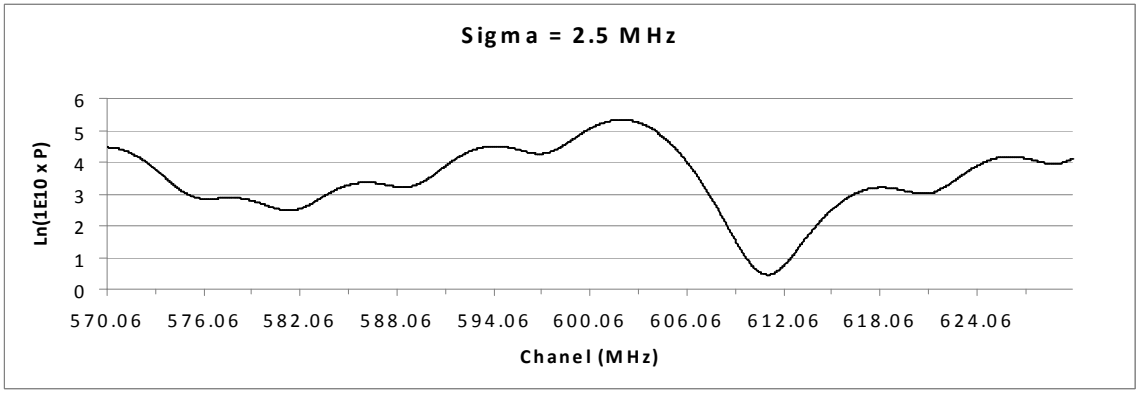


Figure 5.5. Frequency dependence of TV power detected in Hanoi.

## 5.3 Electronics

A general logic diagram of the electronics is shown in Figure 5.6. It includes low noise preamplifiers, one on each antenna, an adder, a filter, a super heterodyne unit (local oscillator and mixer with a 30 MHz filtered output), two amplifiers and a detector unit (amplification, rectification and DC amplification). The electronics is installed in a small case allowing for its easy transport. Low voltage (±15 V) supplies are included and powered from the line (220V/50Hz). A picture of the assembly is shown in Figure 5.7. The antennas are connected via two 50 Ω coaxial cables and the detector output is connected to a DC to frequency converter followed by a scaler read out by a PC under LabView.

### *5.3.1 RF front end*

The antennas are equipped with low noise preamplifiers having a gain of 20 dB for frequencies between 450 and 900 MHz (so-called TV band IV). They are supplied with ±15 V DC via the very same coaxial cables used to transmit the signals received on the antennas. “Polarization T’s” separate DC and RF.

Measurements have been made in the lab using a KEITHLEY 2920 RF generator and an ANRITSU MS2663C spectrum analyzer having dynamic ranges of the order of 10 kHz to 10 GHz. We recall that by definition 0 dBm=1 mW. The power is expressed as a function of impedance $Z$ and wave amplitude $V$ as $P= ½V^2/Z= V^2_{eff}/Z$ where $V_{eff}=V/\sqrt{2}$. Under 50 Ω, 0 dBm (meaning 1 mW) correspond therefore to $V_{eff}=225\ mV$ or $V=316\ mV$ (632 mV peak to peak). The spectrum analyser measures directly $V_{eff}$.

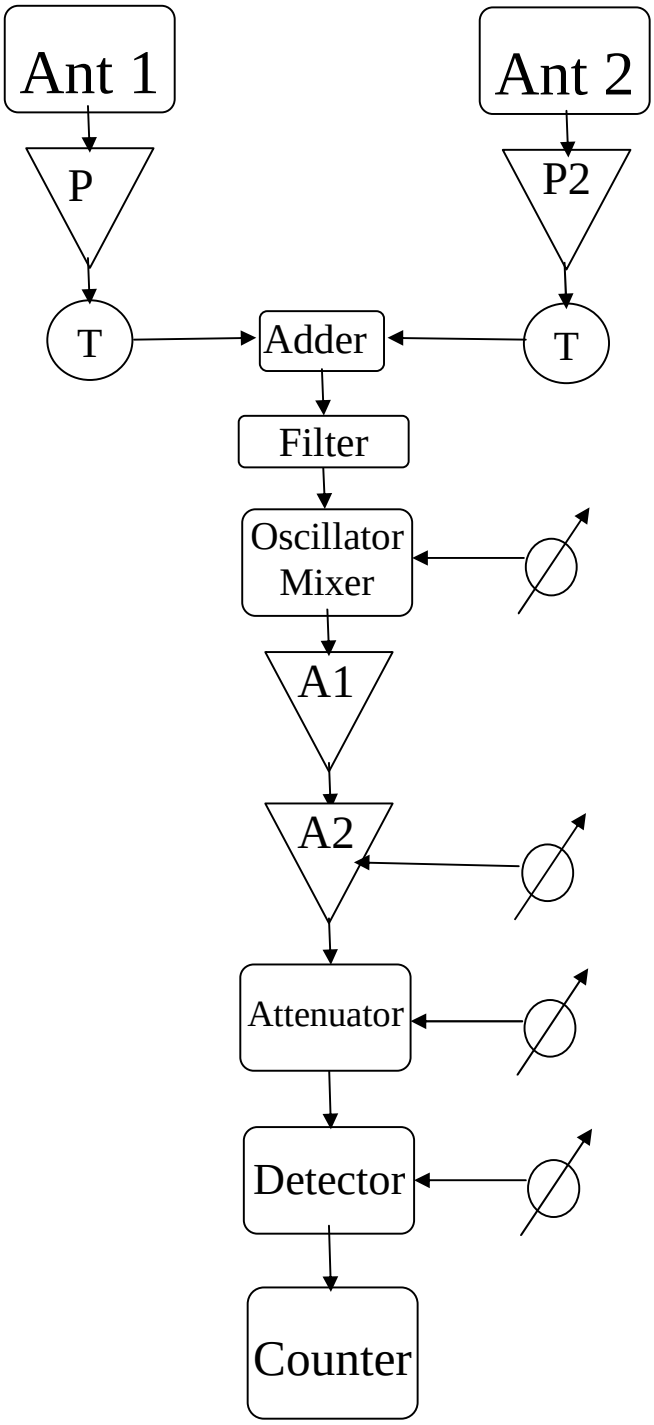


Figure 5.6. Logic diagram of the electronics showing the antennas (Ant), preamplifiers (P), filter, super heterodyne (Oscillator-Mixer), amplifiers (A), variable attenuator, detector and counter. Circles with arrows indicate adjustments (VCO frequency, A2 gain, attenuation and detector range).

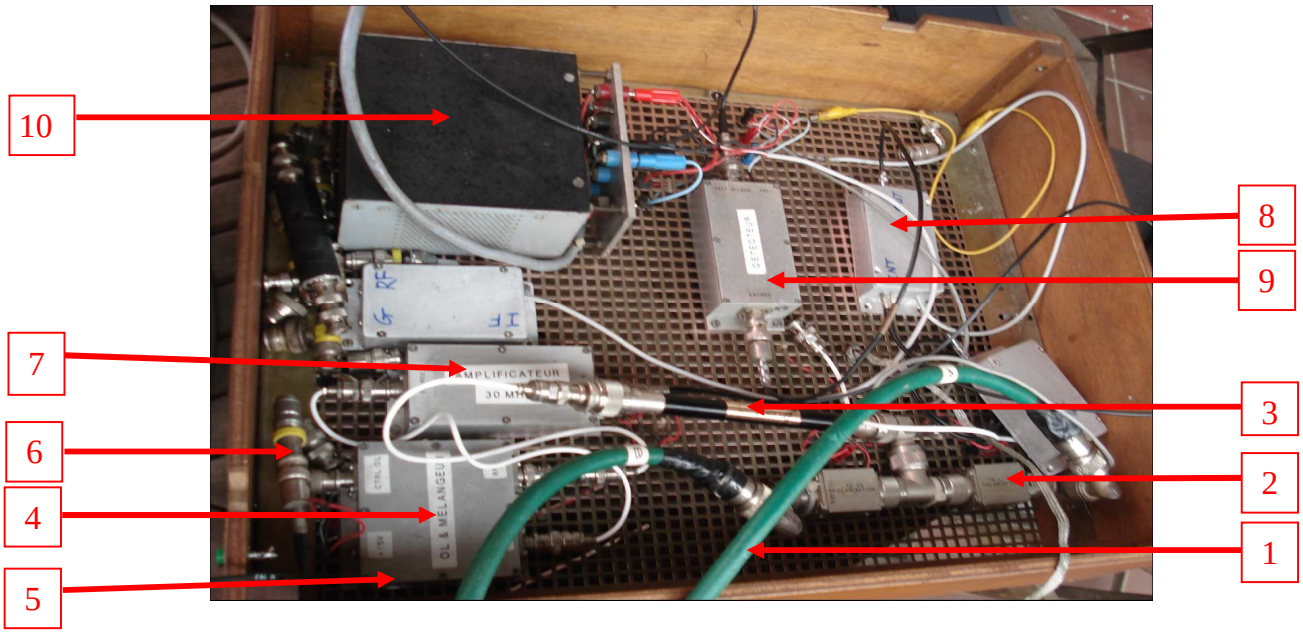


Figure 5.7: Photograph of the electronics assembly: input cable (1), polarization tee (2), 610MHz filter (3), oscillator-mixer (4), VCO adjust (5), VCO frequency monitor (6), 30 MHz amplifier A1 (7), 30 MHz amplifier A2 (8), detector (9) and low voltage power supply (10).

The preamplifier responses reveal a gain difference between the two preamplifiers of 1.0 dB in power (a factor $r=1.12$ in amplitude). The effect on interferometry being modest, no attempt was made at changing the gains. The linearity of both preamplifiers is excellent: for a response of the form $V_{in}^{n}$, $n=1$ to better than 1%.

The filter is located after the adder. Its response has been measured in the laboratory and is displayed in Figure 5.8 as a function of frequency. It is centred on 611 MHz with a bandwidth of ~±7.5 MHz at 3 dB. It eliminates undesired TV signals at an early stage. It attenuates the signal by 6 dB in power (3 dB in amplitude).

The mixer causes the detected signal (preamplified, added and filtered) to beat with a fixed frequency wave in order to work at lower frequencies where working conditions are much easier and where cheaper components are available. The fixed frequency wave is produced by a ~600 MHz voltage controlled oscillator (VCO). Its frequency can be fine tuned using a potentiometer that adjusts the control voltage $V_{co}$. During measurement, the frequency is continuously monitored with a LEADER LDC-824 frequency meter. The beat frequency, around 30 MHz, is the difference between the beating frequencies. Oscillator and mixer are parts of a same unit.

For an oscillator frequency $f_{VCO}$ and an input frequency $f_{RF}$ the output frequency $f_{IF}$

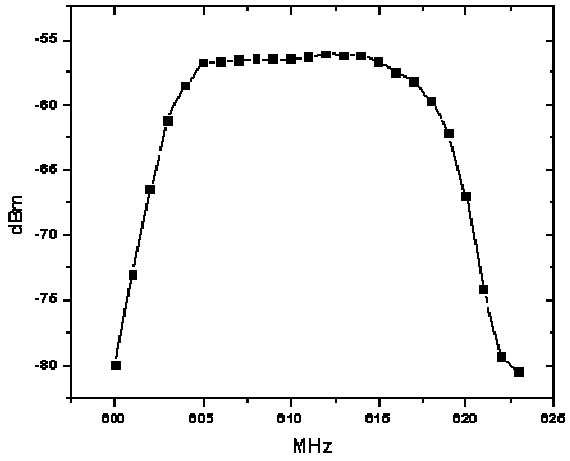


Figure 5.8. Response of the filter as a function of input frequency for –50dBm in.

(called intermediate frequency, IF) is $f_{IF} = f_{RF} - f_{VCO}$. It is filtered at the output stage of the mixer. In quiet conditions, one can tune $f_{VCO}$ using the potentiometer acting on $V_{CO}$ and select this way $f_{RF}$ at will around 610 MHz within the front end filter bandwidth (±7.5 MHz). However, in cases where a strong signal (either fundamental or harmonic) exists at nearby frequencies, it will act on $V_{CO}$ in such a way that the desired frequency cannot be maintained. As we shall see below, this is what happens in the environment of our laboratory.

It turns out that $f_{VCO}$ must exceed 579.4 MHz for stable operation. The bandwidth of the detector is very narrow, of the order of 0.6 MHz centred on 30.4 MHz, well within the bandwidths of the mixer and of the 30 MHz amplifiers. This means that in the absence of strong interferences (stable operation) the detected frequencies are centred on $f_{VCO}+30.4$ *MHz*. In order to stay within the front end filter bandwidth, the detected frequency should not exceed 617 MHz, implying that $f_{VCO}$ should not exceed 586.6 MHz. In practice, for safe operation, one should therefore keep $f_{VCO}$ between 580 and 586 MHz. The data reported below were collected using VCO frequencies between 582.6 and 583.2 MHz. The dependence of $f_{VCO}$ on $f_{RF}$ has been measured in the laboratory and found well behaved.

### *5.3.2 30 MHz amplifiers*

Two 30 MHz amplifiers, A1 and A2 (home made), are used after the mixer. Both have a broad band width. A1 has a fixed gain of 43 dB and the adjustable gain of A2 was set at 20 dB in the set of measurements reported below. Gains and linearities have been measured in the laboratory. An adjustable precision attenuator, set at 3 dB during normal measurements, was inserted between A2 and the detector to allow for an easy calibration of the latter.

### *5.3.3 Detector*

The front end part of the detector unit (Figure 5.9) is made of two amplifiers bracketing a filter, the detector proper being made of a backward diode acting as a rectifier followed by an operational amplifier giving up to ~8 V DC out. The gain of the first amplifier can be varied using a potentiometer of resistance $\rho$ adjustable between 0 and 110 kΩ. Once $\rho$ is set, the dynamic range of the detector is fixed, typically 12 mV to 18 mV for $\rho$ =1 kΩ and 2mV to 6 mV for $\rho$ =100 kΩ. The output DC voltage of the detector was measured as a function of the amplitude at the detector input for different $\rho$ values (Figure 5.10). The generator frequency was fixed at 613 MHz and the VCO frequency at 582.60±0.04 MHz, giving an intermediate frequency of 30.4 MHz, at the maximum of the response of the system.

In order to use the detector in optimal conditions, one has to adjust $\rho$ to obtain an output voltage in the middle of the range, around 4 V. Then, over the narrow window corresponding to the dynamic range of the detector at the value of $\rho$ that has been set, the response is nearly linear. Namely, for an input signal of amplitude *V*, the signal integrated over many IF oscillations is proportional to *V* and not to $V^2$ as would be the case for a square law detector. In particular, in the case of interest here, the signal detected from the Sun and summed over the two antennas shows interference fringes having amplitude much smaller than the underlying background: the associated variations of the detector output voltage stay well within the dynamic range window. However, as we saw earlier, the amplitude of the detected signal is obtained by adding the solar and background signals in quadrature: hence the ratio between their amplitudes being *S/B*, the ratio between the observed oscillations and the background level is essentially $½(S/B)^2$ and, as remarked earlier, the detector behaves as detecting power rather than amplitude.

The bandwidth, measured between 30.0 and 30.6 MHz at 3 dB, is narrower than that of other units and defines therefore the overall bandwidth (Figure 5.11).

Table 5.3 summarizes the gains and bandwidths of the various components of the system.

Table 5.3. Summary of gains and bandwidths

| *Component* | *Gain (dB in power)* | *Bandwidth* |
|---|---|---|
| *Antennas+cables* | *15–4=11* | *broad* |
| *Preamplifiers* | *20/21* | *broad* |
| *Filter* | *–6* | *15 MHz* |
| *Oscillator/Mixer* | *–9* | *6MHz* |
| *Amplifier A1* | *43* | *broad* |
| *Amplifier A2* | *20* | *broad* |
| *Attenuator* | *–3* | *broad* |
| *Detector* | *See Figure 5.11* | *30.0 to 30.6 MHz* |
| *Global* | *76* | *0.6 MHz* |

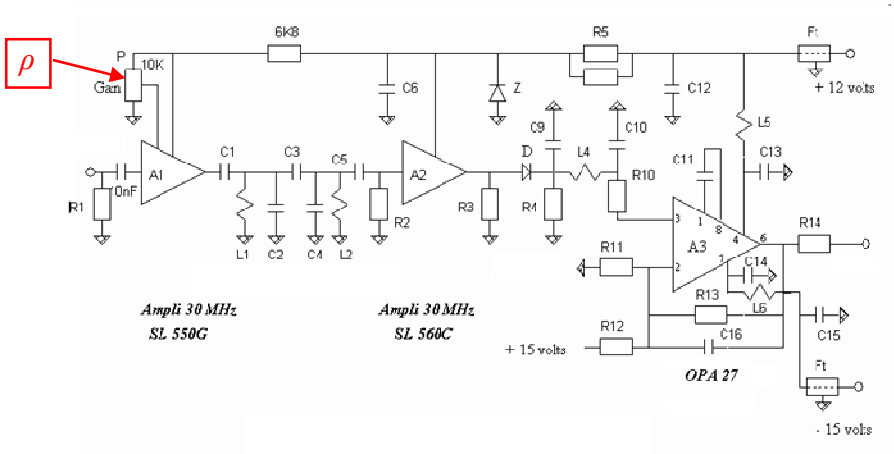


Figure 5.9: Schematic electronic diagram of detector

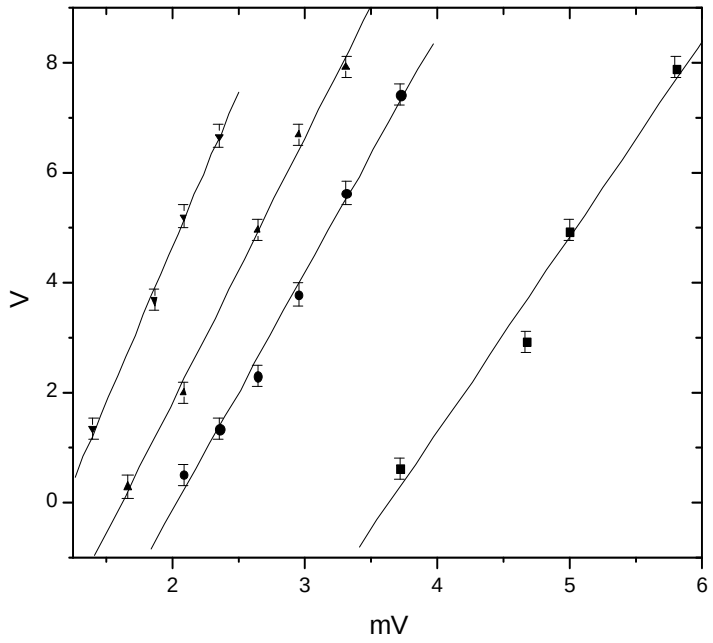


Figure 5.10. Measurement of the detector response for various values of $\rho$.
The detector DC output $V$ (in V) is shown as a function of the amplitude of the 30.4 MHz generator input $v$ (in mV). The fits are of the form $A+Bv$. From right to left:
*$\rho$ =10.0kΩ, A= –12.95±0.65, B= 3.55±0.13 ; $\rho$=30.3kΩ, A=–8.80±0.42, B= 4.33±0.15;*
*$\rho$=50.0kΩ, A= –7.78±0.39, B= 4.81±0.15; $\rho$=104.3 kΩ, A=–6.66±0.56, B= 5.66±0.29 .*

### *5.3.4 Analogue to digital conversion and data acquisition*

The detector DC output is converted to frequency and scaled in a 10 kHz counter which is read out every millisecond into a PC, its content being added to a

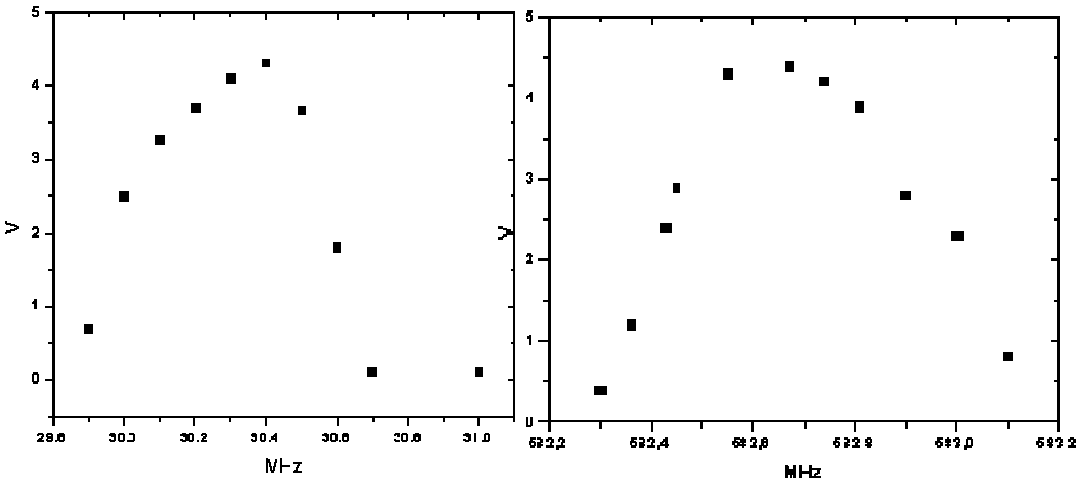


Figure 5.11 Left: lab measurement of the detector bandwidth for –7.6 dBm input corresponding to an amplitude of 4.17 mV. The detector DC output is shown in ordinate (4V correspond to 20'000 counts) and the generator input frequency in abscissa. Right: A 613 MHz RF sine wave from the generator is fed to the oscillator/mixer and the DC output of the detector (in ordinate) is measured as a function of the VCO frequency (in abscissa).

memory which is transferred to the monitoring programme and cleared every second under LabView, providing both storage of the recorded data and on line display of the time dependence.

It is important to read the data as fast as possible to minimize dead time in order to maintain a good duty cycle. The code used to this effect is listed in Appendix. The ADC is read out every ms and its content is added to a memory, the content of which is transferred to the data acquisition under LabView every second or so (the number of measurements per transfer is an adjustable parameter). An on-line display (Figure 5.12) allows for monitoring data taking.


Figure 5.12. Photograph of the online display

# 6. MEASUREMENTS AND RESULTS

## 6.1. Early measurements

The antennas have first been installed on flagpoles on the roof of the laboratory (Figure 5.4). It was soon realized that surrounding emitters in the immediate neighbourhood were producing very strong interference and preventing the detection of solar emission. Attempts at shielding the antennas with a metallic grid acting as a Faraday cage and at shielding the electronics by wrapping its case (Figure 5.7) in aluminium foils have proven unsuccessful. Other sites have been tried near the laboratory but were also found to be polluted by interference and did not allow for a stable operation of the interferometer. It was finally decided to move away from Hanoi to a quieter site.

The site chosen was near Hoa Binh in a region surrounded by hills, in the garden of a private villa. The Sun signal was immediately detected and data have been collected. This early set of measurements proved very useful to understand the detector and become familiar with the analysis of the data. As a result, several features of the detector have been improved. In a first phase, a 8 bit home made ADC was used. It had an integration time (gate) of 100 μs and was equipped with an adjustable pedestal. The data shown in Figure 6.1 were collected on Octorber 28$^{th}$ 2009 between 11:00 and 12:45. The insufficient resolution of the 8 bit ADC is obvious and the fact that the detected signal stays a long time at the same level, without fluctuating, shows that the stability of the equipment allows for a much better resolution.

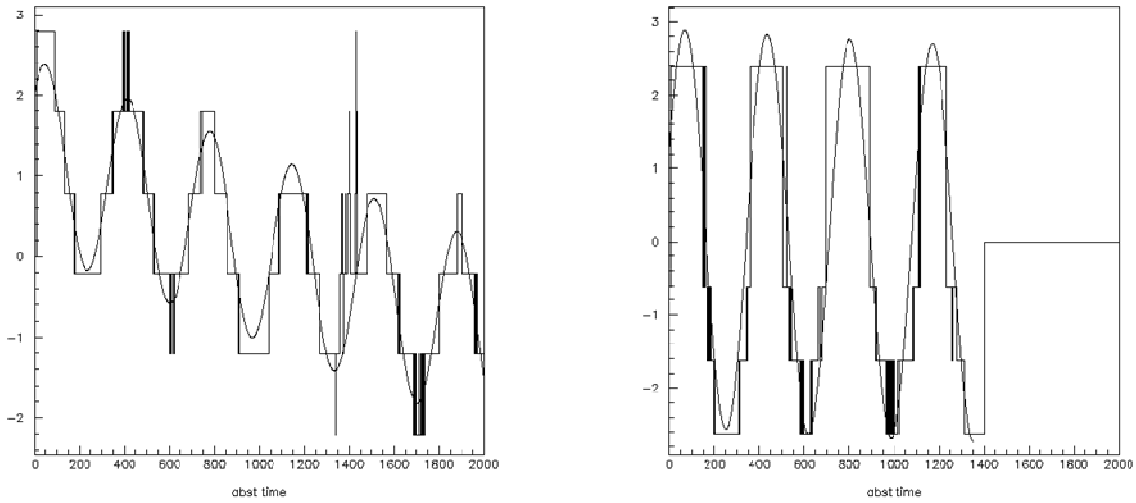


Figure 6.1. Two examples of early measurements (see text).

Another site has been tried in a meteorology station at Tam Dao, providing a nice flat area oriented east-west but facing a close by mobile telephone emitter that made Sun detection again very difficult. It was finally decided to return to Hoa Binh for the final measurements, this time with an improved instrument and better measuring devices.

## 6.2. Observation of interferences

Preliminary measurements have been made in various places in Ha Noi. They have shown the need to work in an electromagnetically quiet place and have given the opportunity to upgrade the detector by adding new components and replacing or fixing old ones. The data presented here were collected in a single day, on June 25$^{th}$ 2010, near Hoa Binh.

Two base lines were used, approximately east-west, with lengths of 22.9±0.1 m (runs 1 to 4) and 17.9±0.1 m (runs 5 to 15) respectively. In both cases the angle with the east-west direction was 4.4±0.7$^{o}$ toward south-east/north-west. The configuration of the ground did not allow for an exactly horizontal base line: the altitude of the western antenna was higher than the altitude of the eastern antenna by 1.56±0.10 m for the 22.9 m base line and 1.44±0.10 m for the 17.9 m base line. Data were collected between ~10:30 am and ~3:45 pm in 15 runs of ~1000 s each. Time and VCO frequency were recorded at the start and at the end of each run.

Shortly after 10 am, with the antennas vertical, the background level was measured and the amplifier, attenuator and detector settings were tuned in such a way as to operate in the middle of the detector linear range, around 22’000 counts. A scan of VCO frequencies did not show any significant frequency dependence of the background level and the system was operated with VCO frequencies between 582.6 and 583.2 MHz. The linearity of the response was measured between –3 dB and +3 dB from the working point with the result that 194 counts correspond to a 1% increase in amplitude (Figure 6.2). The measurement made in the laboratory using a sine wave generator set at 30.4 MHz frequency (Figures 5.10 and 5.11 left) gives a calibration of the detector, 4.3 V DC out (21500 counts) for 4.17 mV in. Averaging over frequency for a uniform frequency distribution at the input of the detector between 29.9 MHz and 30.6 MHz, namely a 0.7 MHz interval, Figure 5.10 gives 15’000 counts for the same 4.17 mV in. Hence, on the working point (22’000 counts meaning 6.12 mV at detector input) 194 counts correspond to 61 μV giving an effective conversion factor of 3.2±0.3 counts per μV, the uncertainty being estimated to be of the order of 10%.

The time dependence of the detected signal is shown in Figure 6.3 for two representative runs, with zero suppressed by 21’500 counts. The run in the left panel displays particularly quiet conditions while the run in the right panel shows evidence for non-linear background conditions. The amplitude of the solar interference is of the

order of ±150 counts, slightly below one percent of the background level. Background fluctuations are usually slow and it was found that using a quadratic time dependence over each particular run was good enough an approximation. Only in one case has it been necessary to disregard a spike that lasted over 40 seconds. The data in the spike

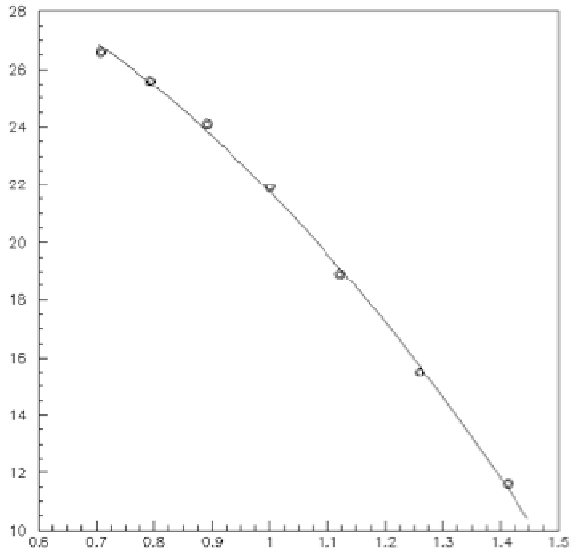


Figure 6.2. Response of the detector. In situ measurement of the linearity of the detector around its working point; the number of counts recorded per second (in ordinate in units of 1000 counts) was measured in the field by changing the setting of the variable attenuator at detector input; the input amplitude, relative to the working point (3dB attenuation, 22'900 counts per second), is shown in abscissa; the curve is the result of a quadratic fit. The detector potentiometer setting was 30.3 kΩ.

range have been replaced by a linear interpolation between data before and after the disturbance. However, small spikes such as that visible on the right panel of Figure 6.3 between 250 s and 300 s have been kept.

The voltage oscillations measured in the antennas are the superposition of RF electric field oscillations having as respective sources the Sun and backgrounds of various origins. Within the bandwidth of the system they add up incoherently – their respective phases being unrelated – and the resulting amplitude of the RF signal is therefore obtained by adding the Sun and background signals in quadrature:

$$S_{det}=\sqrt{(S^2_{Sun}+S^2_{bg})}= (E^2_1\{1+r^2+2r\cos(2\pi D/\lambda)\}+B^2\})^{½}$$
$$\sim B+(E^2_1/B)\{1+r^2+2r\cos(2\pi D/\lambda)\}/2$$

where $B$ is the amplitude of the background and where the second expression is to first order in $E^2_1/B^2$. It is therefore $E^2_1/B^2$ which is at the percent level, implying that $E_1/B$ is at the 10% level.

The data have been compared with the above expression under the assumption that the background term, *B*, could be parameterized as a quadratic function of time during the duration of a given run. In addition to the base line geometry mentioned earlier, the parameters of relevance include the longitude and latitude of the measuring site, $105^o$ 30' E and $20^o$ 53' N respectively, and the declination of the Sun on that day, $23.4^o$. Fits are performed in two steps; in a first step, run dependent parameters are fine-tuned for each run separately by fixing parameters that are common to all runs; in a second step, a global fit is made to all runs together, fixing the run dependent parameters to their former best fit values and fitting parameters that are common to all runs. The procedure is repeated iteratively and a single iteration is found to be sufficient. Run dependent parameters include three parameters describing a quadratic background and a time off-set allowing for a fine tuning of the start time.

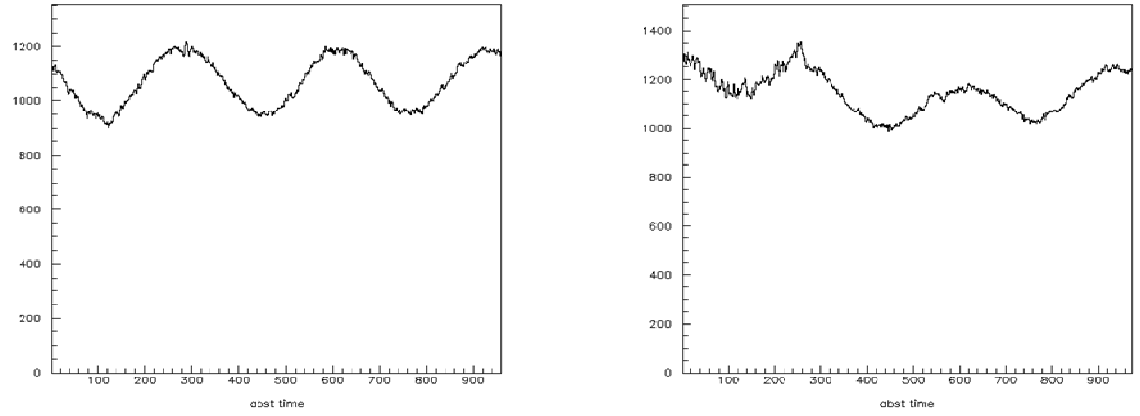


Figure 6.3. Two representative runs. The time, in seconds, is shown in abscissa; the number of counts per second, after subtraction of 21'500 counts, is shown in ordinate.

Global parameters include two parameters describing the orientation of the baseline and the amplitude of the solar fringes. The background level that has been fit to each run independently is taken with reference to a slowly varying component illustrated in Figure 6.4 and described by a form $B_0=23+0.0279(t–5.20)^2$ where *t* is the time measured in minutes from noon. It is therefore described as $B=B_0+\Delta B$ where $\Delta B$ is a run dependent quadratic function of time. For each individual run, the rms value of $\Delta B$ with respect to its mean has been used as a common uncertainty assigned to each measurement of this particular run. In practice, uncertainties were set to $1.8\Delta B$ in order to have a $\chi^2$ of 1 unit per degree of freedom. The fine-tuning of the baseline orientation gave minor shifts with respect to the measured values. The best-fit value of the signal is 1439 counts. In order to obtain an estimate of the uncertainty, dominated by the lack of precise knowledge of the background, individual run fits have been repeated, this time fitting not only the four run-dependent parameters mentioned earlier but also the

amplitude of the signal, the mean and rms values of which are found to be 1483 and 157 counts respectively. The results of the final global fit are shown in Figure 6.6 for each of the 15 runs. The agreement is excellent.

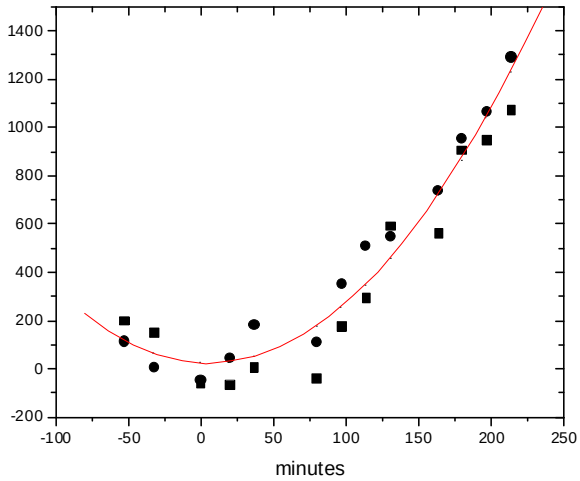


Figure 6.4 Slowly varying background obtained from preliminary linear background fits. The levels at the beginning (squares) and at the end (circles) of each run are shown together with the result of a quadratic fit (curve). Time, measured from noon in minutes, is shown in abscissa. Counts per second are shown in ordinate after subtraction of 21'500 counts.

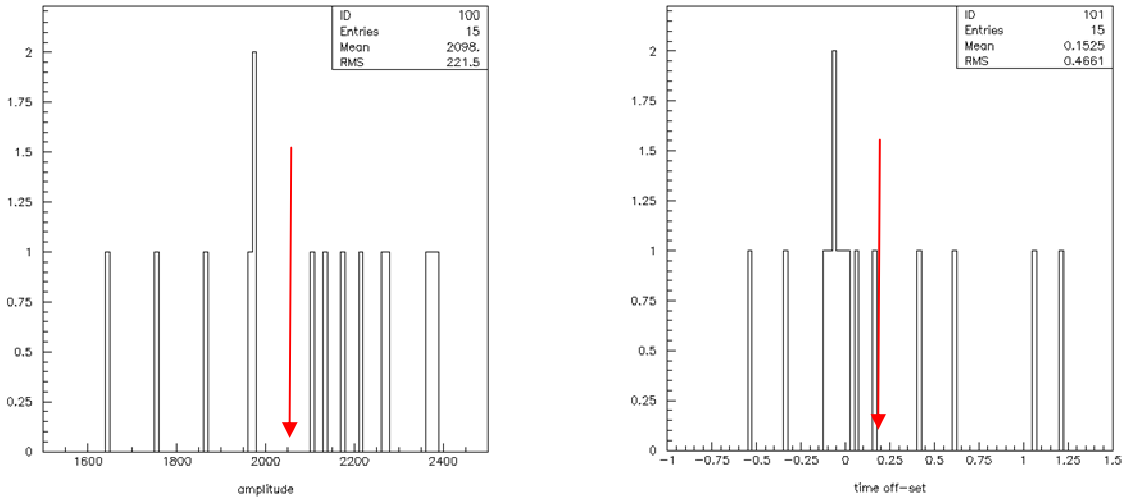


Figure 6.5. Left: Distribution of the signal amplitudes (in number of counts multiplied by √2) obtained from fits made to each run separately. The rms of the distribution (222=157√2 counts) is used as a measure of the global uncertainty. Right: Distribution of the time offsets (in minutes) obtained from the run-by-run fits. Their mean value is 0.16 mn and their rms 0.47 mn.
Arrows indicate the mean values.

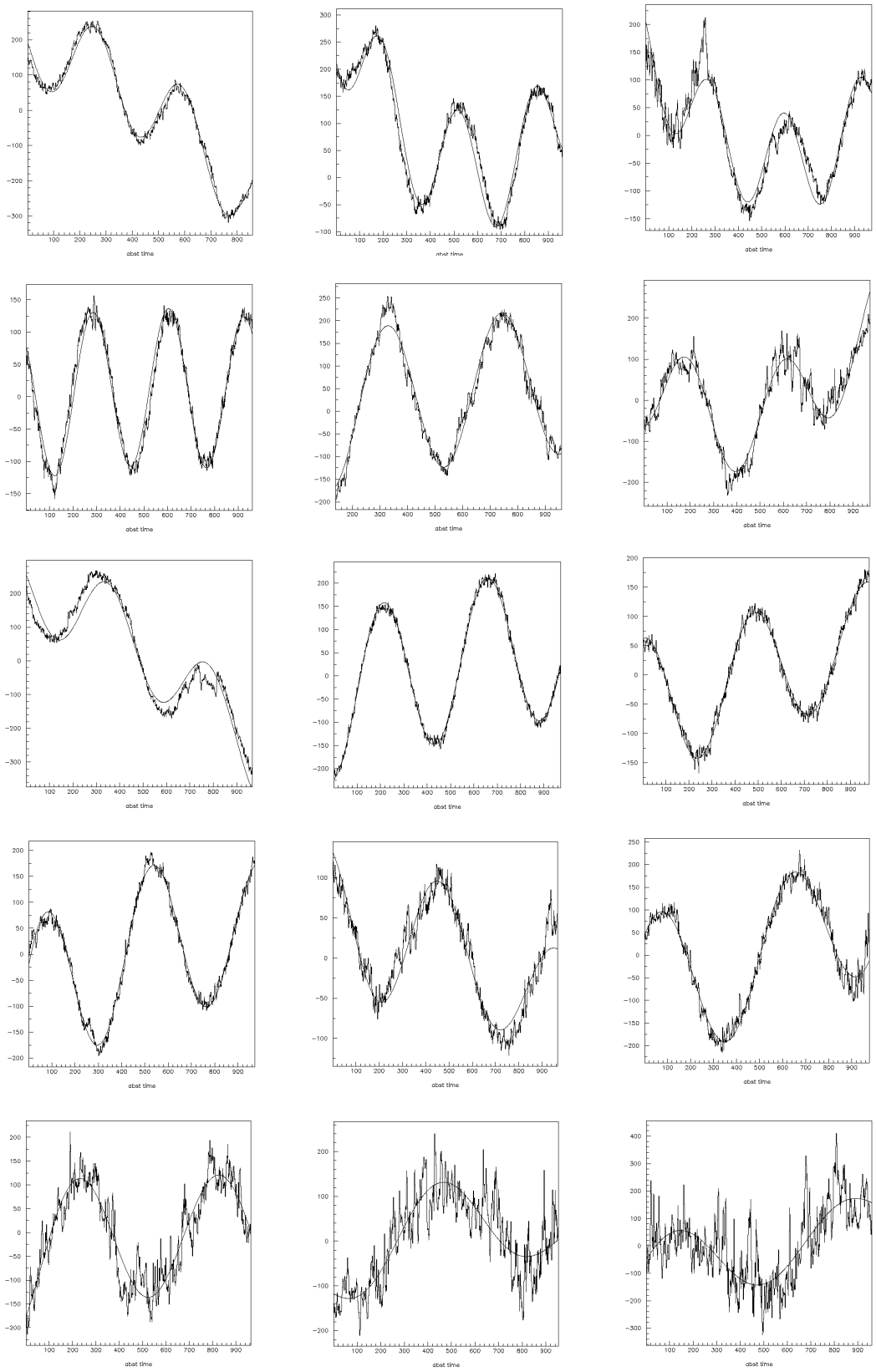


Figure 6.6. Result of the global fit to the measurements of the 15 runs (see text).

### 6.3 Estimate of the solar flux

While the primary aim of the observation was a study of the solar interference fringes, an estimate of the solar flux density has also been obtained. Using the calibration constant of 3.2 counts per μV, we obtain the amplitude of the solar signal at the input of the detector, 450±50 μV, which, under 50 Ω, corresponds to a power of 2.0±0.5 nW. The quoted uncertainty accounts for the lack of precise knowledge of the background, 157/1439=11%. Dividing by the system gain ($10^{7.6}$), by $\lambda^2/4\pi$ (0.020 $m^2$), by the system bandwidth (0.7 MHz) and multiplying by 2 (two polarizations) we obtain a flux density of (7±2) $10^{-21}$ $W/m^2/Hz$ compared to an average quiet Sun flux of 3 $10^{-21}$ $W/m^2/Hz$. A global uncertainty of ±4 dB, attached to the overall gain of the apparatus (including uncertainties on the antenna gain and on the detector calibration constant), must be added to it. In addition, a small correction is necessary to account for the fact that the Sun is not a point source, as implied in Relation 1, but a disk of uniform luminosity with an apparent diameter of 32 arcmin. Integrating Relation 1 over the Sun disk, $S^2=E_1^2\{1+r^2+2r\int cos(2\pi \boldsymbol{A_1 A_2}.(\boldsymbol{u_0}+\boldsymbol{\varepsilon})/\lambda)d\varepsilon^2 d\alpha/(2\pi\varepsilon^2_{max})\}$ where $\boldsymbol{u_0}$ is the unit vector pointing to the centre of the Sun and $\boldsymbol{\varepsilon}$ is a vector normal to it and having azimuth $\alpha$ around it; the integral runs from 0 to $2\pi$ in $\alpha$ and from 0 to $\varepsilon^2_{max}= 22\ 10^{-6}$ in $\varepsilon^2$. The corresponding correction amounts to 15% on average (i.e. 0.6 dB) and has a quadratic dependence on hour angle $H$ of the form $-0.17+3.6\ 10^{-4}\ H+7.5\ 10^{-3}\ H^2$ (Figure 6.7).

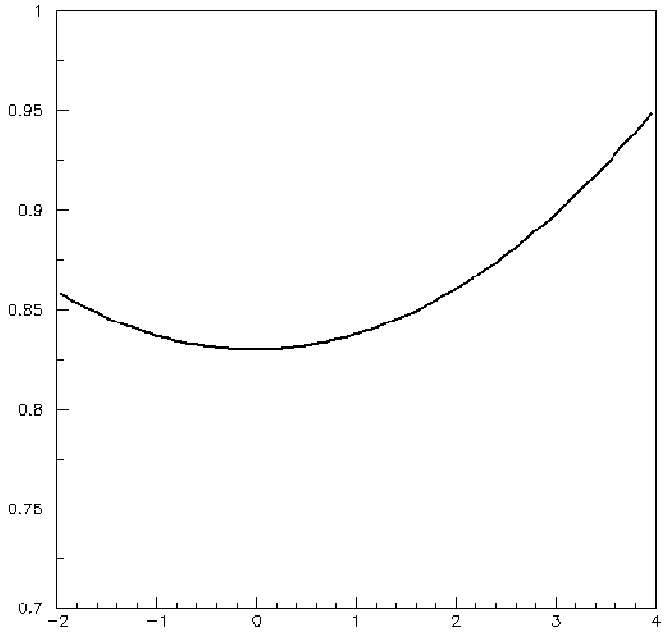


Figure 6.7. Dependence on hour angle (abscissa in hours) of the cosine term smeared by the apparent Sun diameter (see text).

The present estimate of the flux density of the Sun is therefore 4±4 dB above the average emission of the quiet Sun in this frequency range [3]. Indeed, while having long stayed in a quiet state [4], the Sun is now showing signs of entering a new cycle of activity [5]. In particular, on August 1st, 2010, a very strong solar flare (Figure 6.8) has been detected.

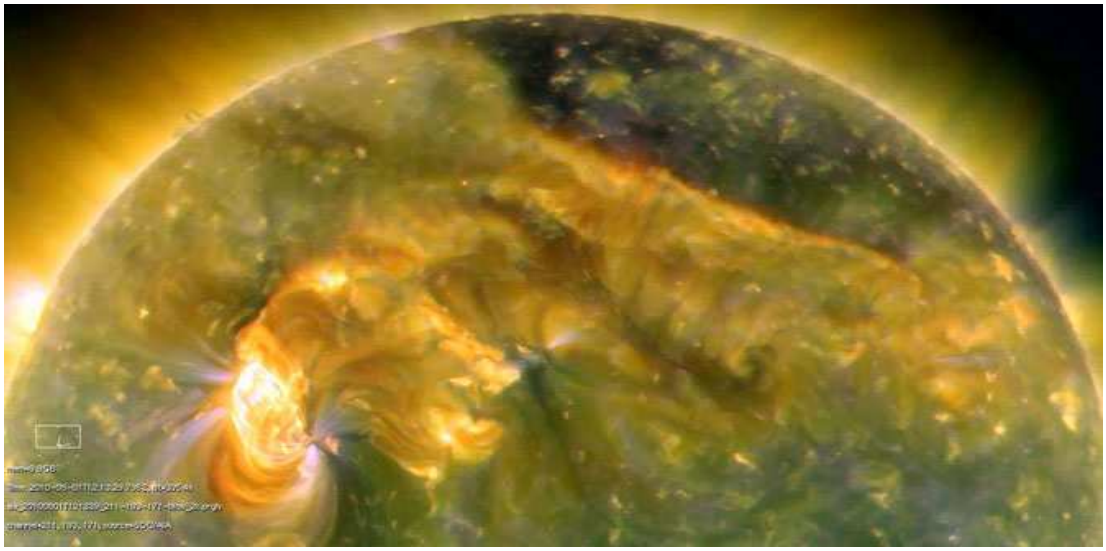

Figure 6.8 (quoted from Reference 5). “On August 1st, almost the entire Earth-facing side of the Sun erupted in a tumult of activity. There was a C3-class solar flare, a solar tsunami, multiple filaments of magnetism lifting off the solar surface, large scale shaking of the solar corona, radio bursts, a coronal mass ejection, and more. This extreme UV snapshot from the Solar Dynamics Observatory (SDO) shows the Sun northern hemisphere in mid eruption. Different colour in the image represent different gas temperatures ranging from to ~1 to ~2 million Kelvin.”

## 6.4 Conclusion and perspective

While having successfully achieved the task of observing radio interference fringes from the Sun, after fifteen years of hibernation, the present work has been mostly an achievement in terms of training. It has given an opportunity to a whole research team, whose expertise is in cosmic ray physics, to gain some familiarity with the methods and techniques of radio astronomy. The quality of the data displayed in Figure 6.6 and the large signal to noise ratio imply that sources with an antenna temperature two orders of magnitude below that of the Sun could be detected with some effort using the same instrument with minor upgrades and improvements. This initiation to radio astronomy has motivated our research team, and more specifically two of us, to pursue their research work in this direction. The laboratory will acquire a small radio telescope equipped for observation of the 21 cm hydrogen line and having a parabolic dish of 2.3 m diameter. We will install it, make it work, and use it to observe hydrogen in the Milky Way and to look again, this time in much greater

details, at the Sun which seems to be waking up and can be expected to be very active in the few years to come. As valuable as they are, however, such observations are of mostly training value and are unable to provide material for real research in modern radio astronomy. This requires much larger instruments available to the international community, such as the VLA. In parallel with the work in Hanoi, we will therefore collaborate with radio astronomers working on such instruments. The presence in Hanoi, close to our laboratory, of Professor Dinh Van Trung who has outstanding experience in radio astronomy, will be an invaluable asset for our efficient training. A collaboration with Professor Frederic Boone, in Toulouse (France), on data collected at the millimetre array of the Plateau de Bure, is also being set up. We very much hope to get support from the Vietnamese scientific community in such a pioneering endeavour.

## References


1. Francois Biraud, Observatoire de Paris, section de Meudon, *La Radioastronomie d'Amateur, une réalisation facile pour amateur,* Astronomie, Novembre 1985, 529.
2. Nguyen Quang Rieu,. *Simple Instruments in Radio Astronomy*. Astronomy for Developing Countries, IAU Special Session at the 24th General Assembly, 2001, Alan H. Batten, ed.
3. J. D. Kraus, Radio astronomy, Mc Graw-Hill Inc, New York, 1966.
4. http://prop.hfradio.org/
5. http://www.nasa.gov/topics/solarsystem/sunearthsystem/main/News080210-cme.html

Chapters 1 to 4 have been written using as sources lecture notes by Professor Pierre Darriulat and information available from the following web sites:

6. http://www.etsu.edu/physics/bsmith/chandra/chandra.html
7. http://www.nastro.org.uk/portal/sun.htm
8. http://schools-wikipedia.org/wp/s/Star.htm
9. http://en.wikipedia.org/wiki/Sun
10. http://wso.stanford.edu/#MeanField
11. http://commons.wikimedia.org/wiki/Commons:Picture_of_the_Year/2006
12. http://www.haystack.mit.edu/edu/undergrad/materials/tut6.htm
13. http://www.nrao.edu/index.php/learn/radioastronomy/radiowaves
14. http://www.cv.nrao.edu/course/astr534/Tour.html
15. http://www.ras.ucalgary.ca/SKA/science/node16.html

# APPENDIX: DATA ACQUISITION CODE

```
#include <stdio.h>
  #include <math.h>
  #include <stdlib.h>
  #include <regan21.h>
  #include <string.h>
  #include <absacc.h>
  #include <Extra-RegEZUSB.h>

  #define uchar unsigned char
  #define uint unsigned int
  #define ulong unsigned long
  #define XBY XBYTE
  #define DBY DBYTE

  xdata uint second _at_ 0x1250;
  xdata uint count _at_ 0x1252;
  xdata uint fdata[1001] _at_ 0x125C;
  xdata uchar start _at_ 0x1255;
  xdata uint preset _at_ 0x1256;
  xdata     uint length _at_ 0x1258;

      void init(void); void Timer2(); void delay(uint j);  void clear(void);

    int visit;
      bit st=0, gd =0;           char s1 [10];
      uint temp = 0, j1 = 0, sec=0;


    void delay(uint j)
    {
      unsigned int i=0,N=j;
      for(i=0;i<j;i++)N--;
    }

      void init(void)
      {
        /* Init USB port */
      XBY[USBCS] = 4 ;
      XBY[ISOCTL]= 1 ;
      XBY[PORTACFG] = 0xFF ;  // Configure some pins of port A as port
      XBY[PORTBCFG] = 0xFF ;  // Configure some pins of port B as port
      XBY[PORTCCFG] = 0xFF ;  // Configure some pins of port C as port and
INT1
      XBY[OEC] = 0xFF ;       // Enable output bit PC4, PC7 of port C
      EA = 1  ;                          /* 1 ENABLE GLOBAL INTERRUPTS */
      T2MOD  = 0x00 ;
      T2CON  = 0x80 ;                   /* INIT TIMER 2 */
      RCAP2L = 0xAF ;
      RCAP2H = 0x3C ;
      TL2 =  RCAP2L ;                    /* load 65535 - 50000 to timer2
and 20 interrupts count 1 second */
```

```
      TH2 =  RCAP2H ;

      ET2 = 1 ;                          /* ENABLE TIMER2 INTERRUPT */
      TR2 = 0 ;                    /* 1 START TIMER2 */

      TMOD = (TMOD & 0xf0) | 0x05;
     TR0 = 0 ;                                /* 1 start counter0 */
      }

      void Timer2() interrupt 5
      {
        visit++ ;
        if(visit >= 40){second++ ; visit = 0 ; sec++;
          if(st==1){XBY[0x1252] = TH0 ;
          XBY[0x1253] = TL0;
          TL0 = 0; TH0 = 0;
            j1++ ; fdata[j1] = count-65000; st=0; length++; }
          if(sec >=preset){ sec =0; st=1; TL0=0; TH0=0;}
          }
        TF2 = 0 ;
      }

      void clear(void)
       {
         int i;
         for(i=0;i<=1000;i++)fdata[i]=0;
         second=0; sec=0;
         j1=0; preset = 1; length=0;
         st=0; TH0=0; TL0=0;
       }

      void main(void)
      {
       int i=0;
       init();
      clear();
       delay(100);
       while(1)
          {
               switch(start)
                     {
                                    case 1 : TR2 = 0; TR0 = 0; start=0;
break ;
                                    case 2 : TR2 = 1; TR0 = 1; start=0;
break ;
                                    case 3 : clear(); start=0; break ;
                                    case 4 : start=0; break ;

                    }


             if (j1>=1000){clear();}
             }
      }
```